AD-A184 473 A STUDY OF SCATTERING FROM E-PLANE CIRCUIT ELEMENTS(U) 1/2
TEXAS UNIV AT AUSTIN MICROWAVE LAB Q ZHANG ET AL.
MAY 87 MW-87-P-5 ARO-21438.37-EL DAAG29-84-K-0076
UNCLASSIFIED F/G 9/1 NL

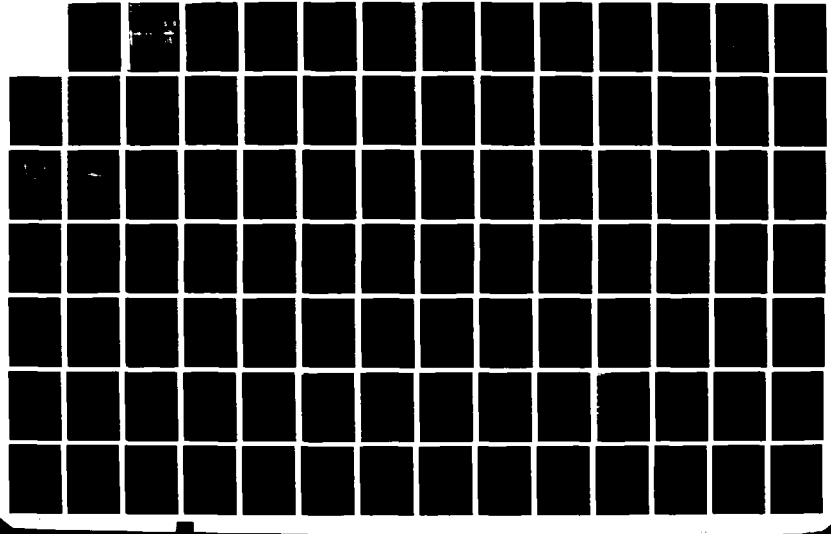

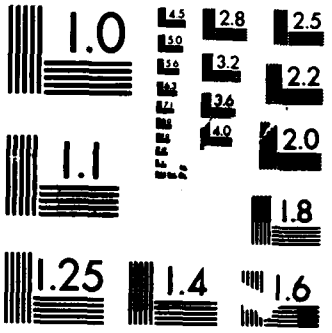

MICROCOPY RESOLUTION TEST CHART
NATIONAL BUREAU OF STANDARDS-1963-A

DTIC FILE COPY

ARO 21438.37-EL

(2)

AD-A184 473

MICROWAVE LABORATORY REPORT NO. 87-P-5

A STUDY OF SCATTERING FROM E-PLANE CIRCUIT ELEMENTS

DTIC
ELECTE
SEP 17 1987
S D

TECHNICAL REPORT

QIU ZHANG AND TATSUO ITOH

MAY 1987

ARMY RESEARCH OFFICE

CONTRACT DAAG 29-84-K-0076

UNIVERSITY OF TEXAS

DEPARTMENT OF ELECTRICAL ENGINEERING

AUSTIN, TEXAS 78712

APPROVED FOR PUBLIC RELEASE

DISTRIBUTION UNLIMITED

87 9 9 234

SECURITY CLASSIFICATION OF THIS PAGE (When Data Entered)

REPORT DOCUMENTATION PAGE		READ INSTRUCTIONS BEFORE COMPLETING FORM
1. REPORT NUMBER Microwave Laboratory Report No. 87-P-5	2. GOVT ACCESSION NO. A184 473	3. RECIPIENT'S CATALOG NUMBER
4. TITLE (and Subtitle) A Study of Scattering from E-Plane Circuit Elements		5. TYPE OF REPORT & PERIOD COVERED technical report 6. PERFORMING ORG. REPORT NUMBER
7. AUTHOR(s) Qiu Zhang and T. Itoh		8. CONTRACT OR GRANT NUMBER(s) DAAG 29-84-K-0076
9. PERFORMING ORGANIZATION NAME AND ADDRESS Dept. of Electrical & Computer Engineering University of Texas Austin, TX 78712		10. PROGRAM ELEMENT, PROJECT, TASK AREA & WORK UNIT NUMBERS
11. CONTROLLING OFFICE NAME AND ADDRESS		12. REPORT DATE May 1987 13. NUMBER OF PAGES 102
14. MONITORING AGENCY NAME & ADDRESS(if different from Controlling Office)		15. SECURITY CLASS. (of this report) 15a. DECLASSIFICATION/DOWNGRADING SCHEDULE

16. DISTRIBUTION STATEMENT (of this Report)

17. DISTRIBUTION STATEMENT (of the abstract entered in Block 20, if different from Report)

18. SUPPLEMENTARY NOTES

19. KEY WORDS (Continue on reverse side if necessary and identify by block number)

evanescent mode filter
waveguide filter
microwave filter

20. ABSTRACT (Continue on reverse side if necessary and identify by block number)

This study contains two parts. In part one, a new analytical technique is introduced to characterize the scattering phenomena of a number of planar E-plane obstacles. This technique is based on the spectral domain method combined with residue calculus. This is the first time the spectral domain method has been used to solve a waveguide excitation problem. It provides some attractive features. For instance, it can handle a wide non-touching E-plane fin on a dielectric substrate; the method deals with inhomogeneous algebraic equations instead of integral equations; and also the spectral domain Green's

DD FORM 1 JAN 73 1473 EDITION OF 1 NOV 65 IS OBSOLETE
S/N 0102-014-6601

SECURITY CLASSIFICATION OF THIS PAGE (When Data Entered)

20. (cont'd.)

functions have simple closed-form expressions. The calculated results for a simplified case are compared with existing data, and are in good agreement. Several curves, useful for E-plane configurations, are included.
Part two presents an analysis and design of an evanescent mode bandpass waveguide filter with non-touching E-plane fins. The theoretical analysis is based on the generalized scattering matrix technique in conjunction with the spectral domain approach, which is described in part one, and mode matching method. The method used in this study takes into account the dominant as well as the higher order mode effects. The measured filter responses in Ka band (26.5-40.0 GHz) are in good agreement with those obtained by this analysis.

QUALITY INSPECTED 2

Accesion For	
NTIS CRA&I	☒
DTIC TAB	☐
Unannounced	☐
Justification	
By	
Distribution /	
Availability Codes	
Dist	Avail and / or Special
A-1	

MICROWAVE LABORATORY REPORT NO. 87-P-5

A STUDY OF SCATTERING FROM E-PLANE CIRCUIT ELEMENTS

TECHNICAL REPORT

QIU ZHANG AND TATSUO ITOH

MAY 1987

ARMY RESEARCH OFFICE

CONTRACT DAAG 29-84-K-0076

UNIVERSITY OF TEXAS

DEPARTMENT OF ELECTRICAL ENGINEERING

AUSTIN, TEXAS 78712

APPROVED FOR PUBLIC RELEASE

DISTRIBUTION UNLIMITED

TABLE OF CONTENTS

A STUDY OF SCATTERING FROM E-PLANE CIRCUIT ELEMENTS

This study contains two parts. In part one, a new analytical technique is introduced to characterize the scattering phenomena of a number of planar E-plane obstacles. This technique is based on the spectral domain method combined with residue calculus. This is the first time the spectral domain method has been used to solve a waveguide excitation problem. It provides some attractive features. For instance, it can handle a wide non-touching E-plane fin on a dielectric substrate; the method deals with inhomogeneous algebraic equations instead of integral equations; and also the spectral domain Green's functions have simple closed-form expressions. The calculated results for a simplified case are compared with existing data, and are in good agreement. Several curves, useful for E-plane configurations, are included.

Part two presents an analysis and design of an evanescent mode bandpass waveguide filter with non-touching E-plane fins. The theoretical analysis is based on the generalized scattering matrix technique in conjunction with the spectral domain approach, which is described in part one, and mode matching method. The method used in this study takes into account the dominant as well as the higher order mode effects. The measured filter responses in Ka band (26.5-40.0 GHz) are in good agreement with those obtained by this analysis.

PART ONE

SPECTRAL DOMAIN ANALYSIS OF SCATTERING FROM E-PLANE CIRCUIT ELEMENTS

I. INTRODUCTION

Recently, finlines [1,2] and other E-plane structures [3,4,5] have found wide applications in millimeter-wave integrated circuits. Their advantages over conventional microstrip at millimeter wavelengths include: reduced radiation, less stringent tolerances, compatibility with hybrid devices, and ease of transition to standard waveguide. A number of passive, active and non-reciprocal components have been developed with the E-plane technique. One of the key elements for passive E-plane components is the E-plane strip that is inserted in the middle of a waveguide parallel to the E plane, as shown in Fig. I-1. A comprehensive design process of E-plane bandpass filters has been reported [6]. The E-plane fin described in Fig. I-1 is an inductive element. Its equivalent circuit is shown in Fig. I-1(c). The analysis of the E-plane fin connecting the top and bottom walls is relatively straightforward [6], because the problem is two-dimensional. The non-touching E-plane fin described in Fig. I-2 is the more general form. It contains both inductive and capacitive elements, as shown in its equivalent circuit. It is more flexible for design. On the other hand, no extensive and accurate characterizations of non-touched E-plane fins seem to exist. A method based on a variational technique has been introduced for a special case where there is no dielectric substrate inserted in the waveguide [7]. The method in [7] is useful for a narrow strip, because only one current component along the E-plane direction is used and the assumed current distribution is constant in the axial (Z) direction.

This study introduces a new analytical technique to characterize the scattering phenomena of a number of planar E-plane obstacles. For instance, it can handle a wide non-touching E-plane fin on a dielectric substrate. Unlike the method

based on the variational technique, scattering coefficients of the dominant, as well as higher-order, modes can be derived. The incident mode can be either dominant or a higher-order.

The method in this study is an extension of the spectral-domain method commonly used for characterizations of eigenmodes in a transmission line on a multi-layer structure. It is extended to the excitation problem and hence provides a set of algebraic equations corresponding to coupled integral equations that would be derived in the space domain. Compared to the integral equation method, the new technique has a number of advantages. For instance, algebraic equations are easier to handle numerically. Also the spectral-domain Green's functions have simple closed-form expressions. Compared to the variational method [7], the present method is not only more versatile but also is attractive from a computational point of view. In the new method, it is necessary to calculate the eigenvalue of only the particular scattered mode of interest. The variational method requires evaluations of all eigenvalues. Furthermore, the method in [7] assumes that only the TE- modes are scattered. By the nature of the formulation, the present method contains both the TE- and TM- modes in its formulation.

The calculated results for a special case ($\varepsilon_1=\varepsilon_2=\varepsilon_3=1$, See Fig.I-2 (b)) are compared with experimental and computed data in [7] to check accuracy. Several useful curves of normalized input admittance and equivalent circuit element values are presented for a number of different parameters of the structure. Those data are applicable to the design of bandpass filters, diode mounts, and tuning elements of the form described by Konishi [3,4,5].

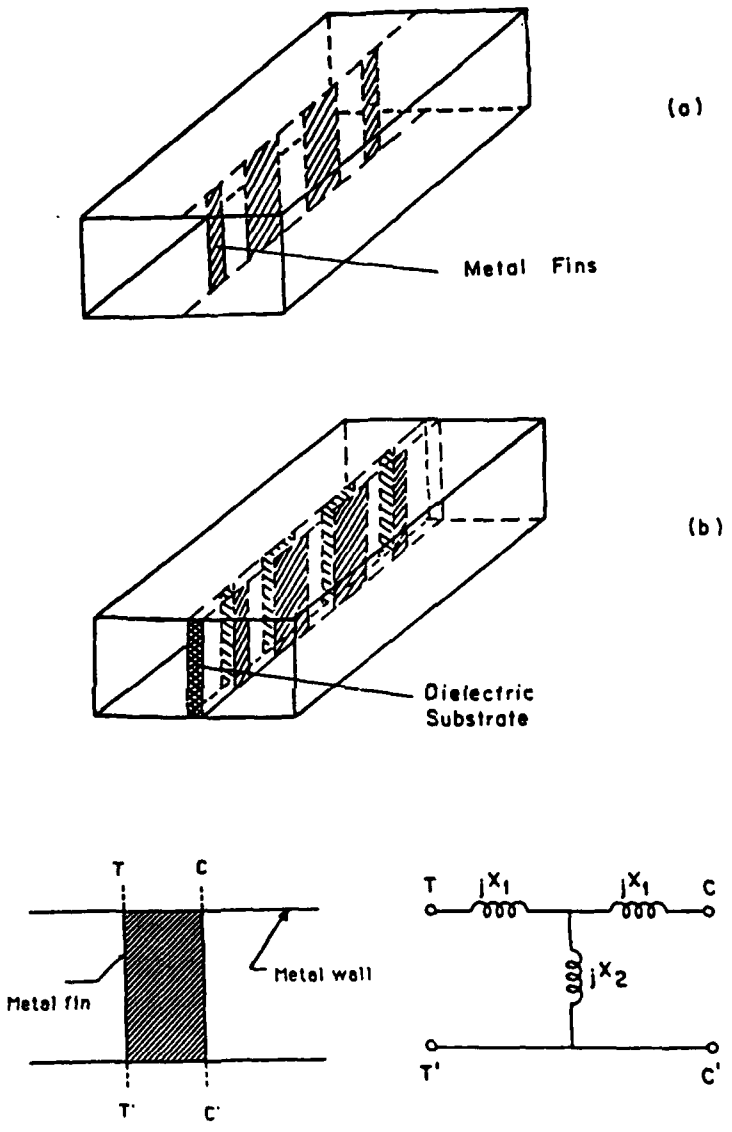

Fig. I-1 E-plan fins in a rectangular waveguide. (a) Metal sheet, (b) Bilateral finline, (c) Metal fin and it's equivalent circuit.

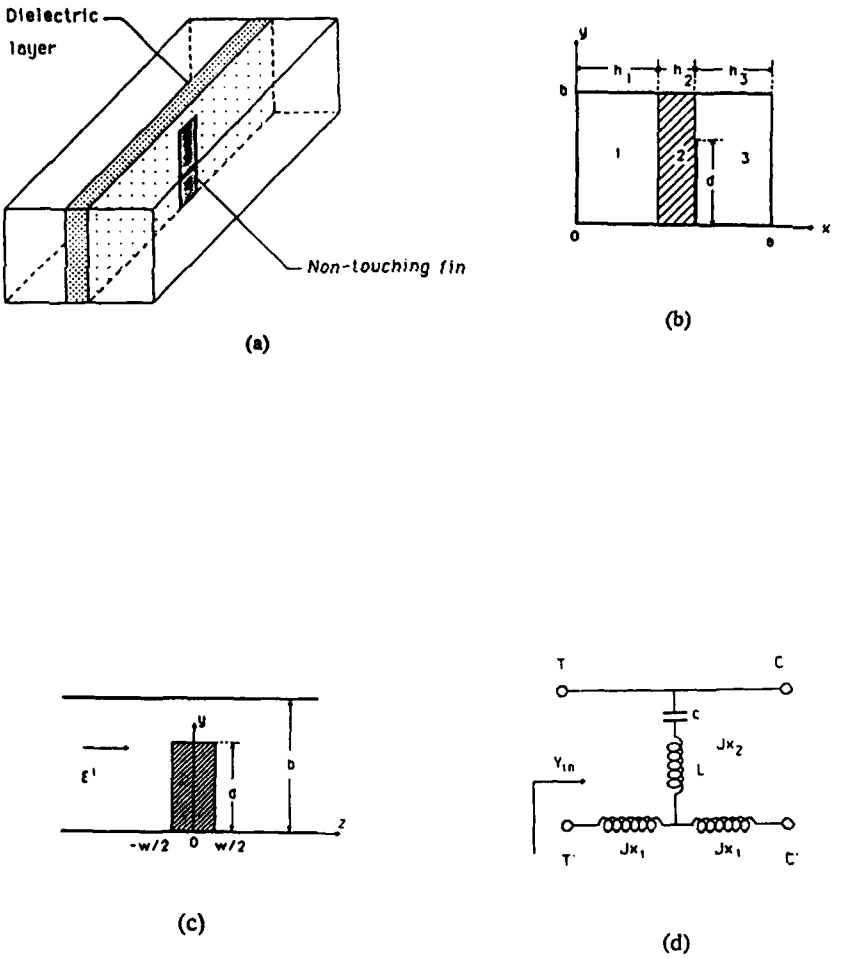

Fig. I-2 (a) non-touching E-plane fin in a rectangular waveguide, (b) End view, (c) Side view, (d) Equivalent circuit ofthe non-touching fin.

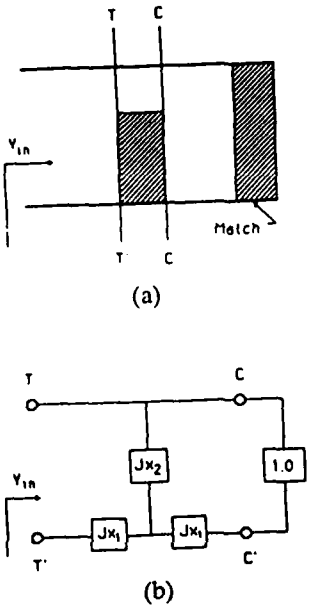

Fig. I-3 (a) An E-plane strip circuit with a matched termination
(b) Two-port equivalent circuit

II. FORMULATION

In this study only the unilateral E-plane fin is treated. Application to a bilateral configuration is straightforward. In reference to Fig. I-2, the strip is assumed to be perfectly conducting and infinitesimally thin. The first step of analysis is to find the scattering parameters at the edge of the non-touching E-plane fin. Then the normalized admittance and other equivalent circuit element values can be obtained from the scattering parameters. The basic idea used in the solution of this problem is described briefly as follows.

For a given incident field E^i, the Fourier transform of the field scattered by the strip, say E_y, can be obtained by using the spectral domain technique. On the other hand, the scattered field E_y can also be written as a sum of the eigenfunctions with unknown coefficients. Taking the Fourier transform of the sum and applying the orthogonality of the eigenfuctions, one determines the unknown coefficients, which are related to the scattering parameters. The non-touchting fin can be expressed by its equivalent circuit. When the waveguide is terminated with a matched load, the values of the equivalent circuit elements are calculated from the real and imaginary parts of the normalized input admittance. The procedure is given in detail below.

A. MODAL EXPANSION OF SCATTERED FIELDS

In this study the harmonic time dependence is the form in $e^{j\omega t}$, but this term is suppressed throughout the analysis for convenience. Consider an incident

electric field E^i which comes from left side of the waveguide as indicated in Fig.I-2, the modal expansion for the E_y component of the scattered field is given by :

$$E_y^S(x,y,z) = E_{y\mathrm{LSE}}^S + E_{y\mathrm{LSM}}^S$$

$$= \begin{cases} \sum_{m=1}^{\infty}\sum_{n=0}^{\infty} C_{mn}^- \phi_m(x)\cos(\alpha_n y)\, e^{j\beta_{mn}(z+W/2)}, & z < -W/2 \\ \sum_{m=1}^{\infty}\sum_{n=0}^{\infty} \phi_m(x)\cos(\alpha_n y)\left(E_{mn}^- e^{j\beta_{mn}z} + E_{mn}^+ e^{-j\beta_{mn}z}\right), & |z| < W/2 \\ \sum_{m=1}^{\infty}\sum_{n=0}^{\infty} C_{mn}^+ \phi_m(x)\cos(\alpha_n y)\, e^{-j\beta_{mn}(z-W/2)}, & z > W/2 \end{cases}$$

$$+ \begin{cases} \sum_{m=1}^{\infty}\sum_{n=1}^{\infty} D_{mn}^- \psi_m(x)\cos(\alpha_n y)\, e^{j\beta'_{mn}(z+W/2)}, & z < -W/2 \\ \sum_{m=1}^{\infty}\sum_{n=1}^{\infty} \psi_m(x)\cos(\alpha_n y)\left(F_{mn}^- e^{j\beta'_{mn}z} + F_{mn}^+ e^{-j\beta'_{mn}z}\right), & |z| < W/2 \\ \sum_{m=1}^{\infty}\sum_{n=1}^{\infty} D_{mn}^+ \psi_m(x)\cos(\alpha_n y)\, e^{-j\beta'_{mn}(z-w/2)}, & z > W/2 \end{cases} \qquad \text{(I-1)}$$

where

$$\phi_m(x) = \begin{cases} C_m \sinh(\gamma_{1m}x), & 0 < x < h_1 \\ A_m \sinh\left[\gamma_{2m}(x-h_1)\right] + B_m \cosh\left[\gamma_{2m}(x-h_1)\right], & h_1 < x < h_1 + h_2 \\ \sinh\left[\gamma_{3m}(a-x)\right], & h_1 + h_2 < x < a \end{cases} \qquad \text{(I-2)}$$

$$\psi_m(x) = \begin{cases} C'_m \sinh(\gamma'_{1m}x), & 0 < x < h_1 \\ A'_m \sinh\left[\gamma'_{2m}(x-h_1)\right] + B'_m \cosh\left[\gamma'_{2m}(x-h_1)\right], & h_1 < x < h_1 + h_2 \\ \sinh\left[\gamma'_{3m}(a-x)\right], & h_1 + h_2 < x < a \end{cases} \qquad \text{(I-3)}$$

and

$$\alpha_n = \frac{n\pi}{b} \qquad \text{(I-4)}$$

$$\alpha_n^2 + \beta_{mn}^2 = k_i^2 + \gamma_{im}^2 \qquad \text{(I-5)}$$

$$\alpha_n^2 + \beta_{mn}'^2 = k_i^2 + \gamma_{im}'^2 \qquad \text{(I-6)}$$

$$k_i = \omega\sqrt{\epsilon_0 \mu_0 \epsilon_i}, \qquad i = 1,2,3. \qquad \text{(I-7)}$$

Here ε_o and μ_o are the permittivity and permeability of free space, respectively; ε_i is the relative dielectric constant in the region i; α_n is the *n*th eigenmode corresponding to the Y direction in the waveguide; γ_{im} and γ'_{im} are the *m*th eigenmodes of LSE- and LSM-modes in the partially filled waveguide in region i, and can be obtained by solving the following eigenvalue equations [8], together with equations (I-5) and (I-6) .

$$\frac{\tanh(\gamma_1 h_1)}{\gamma_1} + \frac{1 + \dfrac{\gamma_3 \tanh(\gamma_2 h_2)}{\gamma_2 \tanh(\gamma_3 h_3)}}{\dfrac{\gamma_3}{\tanh(\gamma_3 h_3)} + \gamma_2 \tanh(\gamma_2 h_2)} = 0 \qquad \text{(I-8)}$$

$$\frac{\gamma'_1 \tanh(\gamma'_1 h_1)}{\varepsilon_1} + \frac{1}{\varepsilon_2} \frac{\dfrac{\gamma'_3 \tanh(\gamma'_3 h_3)}{\varepsilon_3} + \dfrac{\gamma'_2 \tanh(\gamma'_2 h_2)}{\varepsilon_2}}{\dfrac{1}{\varepsilon_2} + \dfrac{\gamma'_3 \tanh(\gamma'_2 h_2) \tanh(\gamma'_3 h_3)}{\gamma'^2_2 \varepsilon_3}} = 0 \qquad \text{(I-9)}$$

where β_{mn} and β'_{mn} are the propagation constants of the *mn*th LSE- and LSM-mode, respectivelty. An equation similar to (I-1) can be written for E_z component . If the induced current components $J_y(y,z)$ and $J_z(y,z)$ are provided the scattered fields E_y^s and E_z^s can be expressed as follows :

$$E_y^S(x,y,z) = \int_0^b dy' \int_{-\infty}^{\infty} dz' \left[Gyy(x, y-y', z-z') J_y(y', z') \right.$$

$$\left. + G_{yz}(x, y-y', z-z') J_z(y', z') \right] \qquad \text{(I-10)}$$

$$E_z^S(x,y,z) = \int_0^b dy' \int_{-\infty}^{\infty} dz' \left[G_{zy}(x, y-y', z-z') J_y(y', z') \right.$$

$$\left. + G_{zz}(x, y-y', z-z') J_z(y', z') \right]. \qquad \text{(I-11)}$$

where G_{yy} etc. are the Green's functions in the space domain. One way to find J_y and J_z is the application of the integral equations which require that the total tangential electric field components to be zero on the strip.

$$E_y^i(x,y,z) + E_y^S(x,y,z) = 0 \qquad \text{(I-12)}$$

$$(x = h_1 + h_2,\ y, z \text{ on strip}).$$

$$E_z^i(x,y,z) + E_z^S(x,y,z) = 0 \qquad \text{(I-13)}$$

The integral equations are

$$E_y^i(h_1+h_2, y, z) + \int_0^b dy' \int_{-W/2}^{W/2} dz' \left[G_{yy}(h_1+h_2, y-y', z-z') J_y(y', z') \right.$$

$$\left. + G_{yz}(h_1+h_2, y-y', z-z') J_z(y', z') \right] = 0 \qquad \left(0 < y < b, |z| < \frac{W}{2}\right)$$

(I-14)

$$E_z^i(h_1+h_2, y, z) + \int_0^b dy' \int_{-W/2}^{W/2} dz' \left[G_{zy}(h_1+h_2, y-y', z-z') J_y(y', z) \right.$$

$$\left. + G_{zz}(h_1+h_2, y-y', z-z') J_z(y', z') \right] = 0 \qquad \left(0 < y < b, |z| < \frac{W}{2}\right).$$

(I-15)

If Eqs. (I-14) and (I-15) are solved, J_y and J_z can be obtained. These J_y and J_z are then substituted into Eqs. (I-10) and (I-11) so that E_y^s and E_z^s are available everywhere. If the scattered field coefficient of a particular mode is needed, the E_y^s and E_z^s can be used in (I-1). Each coefficient may be found using the orthogonality of the expansion functions. Although the above formulation is correct, such an approach is not adopted in this study. Instead, a corresponding procedure is applied in the Fourier-transformed domain. There are two reasons for using this new technique.

(1) In the Fourier-transformed (spectral) domain, coupled algebraic equations instead of coupled integral Eqs. (I-14) and (I-15) are involved.

(2) Derivation of the Green's functions in the space-domain is very complicated. In the spectral-domain, the Fourier-transformed Green's functions are given in closed forms.

The Fourier transform is defined as following:

$$\tilde{F}(\alpha_n, \beta) = \int_{-b}^{b} e^{j\alpha_n y}\, dy \int_{-\infty}^{\infty} f(y, z)\, e^{j\beta z}\, dz$$

$$\alpha_n = \frac{n\pi}{b}. \qquad \text{(I-16)}$$

The Fourier transform of Eq. (I-1) at $x=h_1+h_2$ is given by

$$\tilde{E}_y^S(\alpha_n,\beta) = \tilde{E}_{y\mathrm{LSE}}^S + \tilde{E}_{y\mathrm{LSM}}^S$$

$$= \sum_{m=1}^{\infty} b\delta_n \sinh(\gamma_{3m}h_3)\Bigg\{ C_{mn}^{-}\left[\frac{e^{-jW\beta/2}}{j(\beta+\beta_{mn})} - \pi\delta(\beta+\beta_{mn})e^{j\beta_{mn}W/2}\right]$$

$$+\left[E_{mn}^{-}\frac{\sin\frac{(\beta+\beta_{mn})W}{2}}{(\beta+\beta_{mn})} + E_{mn}^{+}\frac{\sin\frac{(\beta-\beta_{mn})W}{2}}{(\beta-\beta_{mn})}\right]$$

$$+ C_{mn}^{+}\left[\pi\delta(\beta-\beta_{mn})e^{j\beta_{mn}W/2} - \frac{e^{j\beta W/2}}{j(\beta-\beta_{mn})}\right]\Bigg\}$$

$$+ \sum_{m=1}^{\infty} k_n\, b\sinh(\gamma'_{3m}h_3)\Bigg\{ D_{mn}^{-}\left[\frac{e^{-j\beta W/2}}{j(\beta+\beta'_{mn})} - \pi\delta(\beta+\beta'_{mn})e^{j\beta'_{mn}W/2}\right]$$

$$+\left[F_{mn}^{-}\frac{\sin\frac{(\beta+\beta'_{mn})W}{2}}{\beta+\beta'_{mn}} + F_{mn}^{+}\frac{\sin\frac{(\beta-\beta'_{mn})W}{2}}{\beta-\beta'_{mn}}\right]$$

$$+ D_{mn}^{+}\left[\pi\delta(\beta-\beta'_{mn})e^{j\beta'_{mn}W/2} - \frac{e^{j\beta W/2}}{j(\beta-\beta'_{mn})}\right]\Bigg\} \qquad n=0,1,2,\cdots \tag{I-17}$$

where

$$\delta_n = \begin{cases} 2 & n=0 \\ 1 & n\neq 0 \end{cases} \qquad k_n = \begin{cases} 1 & n\neq 0 \\ 0 & n=0. \end{cases}$$

The coefficients $C_{mn}^{\pm}$ and $D_{mn}^{\pm}$ can be solved by the orthogonality of the eigenfunctions, if the scattering field E_y^S is known.

B. SCATTERED FIELDS IN SPECTRAL DOMAIN

Next step is to obtain the scattered fields in the Fourier-transformed domain. To this end, the spectral-domain technique needs to be extended to the excitation problem. The Fourier transform of Eqs. (I-14) and (I-15) at $x=h_1+h_2$ is given by

$$\tilde{E}_y^i(\alpha_n,\beta)+\tilde{E}_y^s(\alpha_n,\beta)=\tilde{E}_y^t(\alpha_n,\beta) \tag{I-18}$$

$$\tilde{E}_z^i(\alpha_n,\beta)+\tilde{E}_z^s(\alpha_n,\beta)=\tilde{E}_z^t(\alpha_n,\beta) \tag{I-19}$$

where

$$\tilde{E}_y^s(\alpha_n,\beta)=\tilde{G}_{yy}(\alpha_n,\beta)\tilde{J}_y(\alpha_n,\beta)+\tilde{G}_{yz}(\alpha_n,\beta)\tilde{J}_z(\alpha_n,\beta) \tag{I-20}$$

$$\tilde{E}_z^s(\alpha_n,\beta)=\tilde{G}_{zy}(\alpha_n,\beta)\tilde{J}_y(\alpha_n,\beta)+\tilde{G}_{zz}(\alpha_n,\beta)\tilde{J}_z(\alpha_n,\beta) \tag{I-21}$$

are the scattered electric fields in the spectral domain. $\tilde{G}_{yy}$, $\tilde{G}_{yz}$, and $\tilde{G}_{zz}$ can be obtained by the immittance approach [9] (Appendix A). Notice that the right sides of Eqs. (I-18) and (I-19) are not zero. This is because the application of the Fourier transform requires use of fields not only on the strip but also the fields outside of tthe strip. Hence, Eqs. (I-18) and (I-19) contains four unknowns $\tilde{J}_y$, $\tilde{J}_z$, $\tilde{E}_y^s$ and $\tilde{E}_z^s$. In the process of solution by Galerkin's method, $\tilde{E}_y^s$ and $\tilde{E}_z^s$ are eliminated. To this end, $\tilde{J}_y$ and $\tilde{J}_z$ are expand as follows:

$$\tilde{J}_y(\alpha_n,\beta)=\sum_{i=1}^{I} a_i\tilde{J}_{yi}(\alpha_n,\beta) \tag{I-22}$$

$$\tilde{J}_z(\alpha_n,\beta)=\sum_{j=1}^{J} b_j\tilde{J}_{zj}(\alpha_n,\beta). \tag{I-23}$$

where a_i and b_j are the unknown current coefficients and need to be determined. The $\tilde{J}_{yi}$ and $\tilde{J}_{zj}$ are basis fuctions. They should be selected in accordance with criteria that will be discussed in the next section. Substituting Eqs.(I-22) and (I-23) into Eqs. (I-18) and (I-19) and taking the inner product of the resultant equations with suitable basis functions, we may use the Parseval's relation to eliminate $\tilde{E}_y^s$ and $\tilde{E}_z^s$. The inner products of $\tilde{E}_y^s$ and $\tilde{J}_{yi}$, and $\tilde{E}_z^s$ and $\tilde{J}_{zj}$ are zero, because $\tilde{J}_{yi}$ and $\tilde{J}_{zj}$ are Fourier transforms of the functions that are nonzero on the strip while $\tilde{E}_y^s$ and $\tilde{E}_z^s$ are transforms of the functions nonzero outside the strip. The results are given by

$$\sum_{i=1}^{I} K_{pi}^{yy} a_i + \sum_{j=1}^{J} K_{pj}^{yz} b_j = -S_{yp}, \qquad p = 1,2,\cdots I \tag{I-24}$$

$$\sum_{i=1}^{I} K_{qi}^{zy} a_i + \sum_{j=1}^{J} K_{qj}^{zz} b_j = -S_{zq}, \qquad q = 1,2,\cdots J \tag{I-25}$$

where

$$K_{pi}^{yy} = \sum_{n=-\infty}^{\infty} \int_{-\infty}^{\infty} \tilde{J}_{yp}^{*}(\alpha_n,\beta)\tilde{G}_{yy}(\alpha_n,\beta)\tilde{J}_{yi}(\alpha_n,\beta)\,d\beta \tag{I-26}$$

$$K_{pj}^{yz} = K_{qi}^{zy}$$

$$= \sum_{n=-\infty}^{\infty} \int_{-\infty}^{\infty} \tilde{J}_{yp}^{*}(\alpha_n,\beta)\tilde{G}_{yz}(\alpha_n,\beta)\tilde{J}_{zj}(\alpha_n,\beta)\,d\beta \tag{I-27}$$

$$K_{qj}^{zz} = \sum_{n=-\infty}^{\infty} \int_{-\infty}^{\infty} \tilde{J}_{zq}^{*}(\alpha_n,\beta)\tilde{G}_{zz}(\alpha_n,\beta)\tilde{J}_{zj}(\alpha_n,\beta)\,d\beta \tag{I-28}$$

$$S_{py} = \sum_{n=-\infty}^{\infty} \int_{-\infty}^{\infty} \tilde{J}_{yp}^{*}(\alpha_n,\beta)\tilde{E}_y^{i}(\alpha_n,\beta)\,d\beta \tag{I-29}$$

$$S_{qz} = \sum_{n=-\infty}^{\infty} \int_{-\infty}^{\infty} \tilde{J}_{zq}^{*}(\alpha_n,\beta)\tilde{E}_z^{i}(\alpha_n,\beta)\,d\beta \tag{I-30}$$

where * indicates the complex conjugate.

For a given incident field, Eqs.(I-24) and (I-25) are solved, and a_i and b_j can be obtained. Hence, $\tilde{J}_y$ and $\tilde{J}_z$ are now known. The scattered fielts in the Fourier-transformed domain, which is described by Eqs. (I-20) and (I-21) , now are completely determined. Since $\tilde{G}_{yy}$, $\tilde{G}_{yz}$, $\tilde{G}_{zz}$, $\tilde{J}_y$,and $\tilde{J}_z$ are all known.

C. SCATTERING PARAMETERS

The scattering coefficients $C_{mn}^{\pm}$ and $D_{mn}^{\pm}$ can now be obtained. Let us express the left-hand side of Eq. (I-16) with Eq. (I-20). Since $\tilde{J}_y$ and $\tilde{J}_z$ are now found, $\tilde{G}_{yy}$ and $\tilde{G}_{yz}$ are given in closed forms: (Appendix A)

$$\tilde{G}_{yy} = Z^e N_z^2 + Z^h N_y^2 \qquad \text{(I-31)}$$

$$\tilde{G}_{yz} = \tilde{G}_{zy} = (Z^e - Z^h) N_z N_y \qquad \text{(I-32)}$$

$$\tilde{G}_{zz} = Z^h N_z^2 + Z^e N_y^2 \qquad \text{(I-33)}$$

where Z^e, Z^h, N_y, and N_z are given in Appendix A. The left-hand side of Eq.(I-17) is completely known. Furthermore, the left-hand side contains poles at $\beta = \pm\beta_{mn}$ and $\beta = \pm\beta'_{mn}$, since they are zeros of the denominators of $\tilde{G}_{yy}$ and $\tilde{G}_{yz}$. These values provide the eigenvalues of the LSE- and LSM-modes, γ_{im} and γ'_{im}. The right-hand

side of (I-17) contains LSE poles at $-\beta_{mn}$ in the C_{mn}^{-} term and at $+\beta_{mn}$ in the C_{mn}^{+} term. It contains LSM poles at $-\beta'_{mn}$ in the D_{mn}^{-} term and at $+\beta'_{mn}$ in the D_{mn}^{+} term. Therefore, $C_{mn}^{\pm}$ and $D_{mn}^{\pm}$ can be obtained by residue calculus. This process corresponds to the use of the orthogonality relationship to find the modal coefficients in the space-domain. The results are given by:

$$C_{mn}^{\pm} = \pm \lim_{\beta \to \pm \beta_{mn}} \left[(\beta \mp \beta_{mn}) \frac{\tilde{G}_{yy}(\alpha_n, \beta)\tilde{J}_y(\alpha_n, \beta) + \tilde{G}_{yz}(\alpha_n, \beta)\tilde{J}_z(\alpha_n, \beta)}{jb\delta_n \sinh(\gamma_{3m} h_3)} e^{\mp jw\beta/2} \right]$$

$$\left(n = 0, 1, 2, \cdots, m = 1, 2, 3 \cdots \delta_n = \begin{cases} 2 & n = 0 \\ 1 & n \neq 0 \end{cases} \right) \qquad \text{(I-34)}$$

$$D_{mn}^{\pm} = \mp \lim_{\beta \to \pm \beta'_{mn}} \left[(\beta \mp \beta'_{mn}) \frac{\tilde{G}_{yy}(\alpha_n, \beta)\tilde{J}_y(\alpha_n, \beta) + \tilde{G}_{yz}(\alpha_n, \beta)\tilde{J}_z(\alpha_n, \beta)}{j\, b \sinh(\gamma'_{3m} h_3)} e^{\mp jw\beta/2} \right]$$

$$(n = 1, 2, 3 \cdots, m = 1, 2, 3 \cdots) \qquad \text{(I-35)}$$

It should be noted that, the above equations are simplified in the case of E-plane fins connecting the top and bottom wall. Since there are no field variations in the y-direction and only TE_{no} modes are scattered for a TE_{10} excitation, we have only one equation (I-18). All the Fourier-transformed quantities are functions of β only.

D. NORMALIZED INPUT IMPEDANCE AND EQUIVALENT CIRCUIT ELEMENTS

The non-touching E-plane fin shown in Fig. I-2(a) may be represented by an equivalent T-network, as shown in Fig. I-2(c). When the waveguide is

terminated with a matched load, as shown in Fig. I-3(a), its equivalent circuit is shown in Fig. I-3(b). The normalized input admittance may be represented by

$$Y_{in} = G_{in} + jB_{in} = \frac{1-R}{1+R} \tag{I-36}$$

where R is the reflection coefficient for the dominant mode, and can be determined in the present method by means of Eqs. (I-34) and (I-35). The normalized reactances X_1 and X_2 can be determined, after Y_{in} in Eqs. (I-34) and (I-35) is obtained. The expressions of X_1 and X_2 are given by Eqs. (I-37) and (I-38). (APPENDIX B)

$$X_2 = \pm\left[\left(\frac{B_{in}}{B_{in}^2+G_{in}^2-G_{in}}\right)^2 + \frac{G_{in}-1}{B_{in}^2+G_{in}^2-G_{in}}\right]^{1/2} \tag{I-37}$$

$$X_1 = \frac{B_{in}}{G_{in}-\left(B_{in}^2+G_{in}^2\right)} \mp X_2. \tag{I-38}$$

The sign in Eqs.(I-37) and (I-38) can be determined by using the Foster reactance theorem which require $dx/d\omega > 0$ for a lossless element. We can also determine the values of C and L in the equivalent circuit Fig. I-3(b), once X_2 is found, under the assumption that the variations of C and L with frequency are small. The capacitance and inductance can be obtained by solving coupled equations.

$$\omega L - \frac{1}{C\omega} = X_2 \tag{I-39}$$

$$L + \frac{1}{C\omega^2} = \frac{dX_2}{d\omega}. \tag{I-40}$$

III RESULTS AND DISCUSSION

A. CHOICE OF BASIS FUNCTION

In principle any kind of basis functions may be used as long as it is nonzero only on the strip. However, due to the variational nature of the spectral domain method, the efficiency and accuracy of this approach depends greatly on the choice of basis functions. For rapid convergence of the solution, the functions should satisfy the edge condition [10]. Also it is desirable that the Fourier transforms of the basis functions are available in a analytical form. With the above consideration, the following set of functions are employed.

$$J_{yl}(y,z) = \frac{\cos\left[(k-1)\left(\frac{\pi z}{W}+\frac{\pi}{2}\right)\right]}{\sqrt{1-\left(\frac{2z}{W}\right)^2}} \frac{\sin\left[(2l-1)\left(\frac{\pi y}{2d}+\frac{\pi}{2}\right)\right]}{\sqrt{1-\left(\frac{y}{d}\right)^2}} \qquad \text{(I-41)}$$

$$J_{zj}(y,z) = \frac{\sin\left[k\left(\frac{\pi z}{W}+\frac{\pi}{2}\right)\right]}{\sqrt{1-\left(\frac{2z}{W}\right)^2}} \frac{\cos\left[(2l-1)\left(\frac{\pi y}{2d}+\frac{\pi}{2}\right)\right]}{\sqrt{1-\left(\frac{y}{d}\right)^2}} \qquad \text{(I-42)}$$

where k and l are integers, and i and j are given by a suitable combination of k and l. The basis function $J_{y1}(y,z)$ ($l=1$ and $k=l$) is shown in Fig. I-4(a); and $J_{z1}(y,z)$, corresponding to $l=1$ and $k=2$, is expresed in Fig. I-4(b). The Fourier transforms of the basis functions are given by Eqs. (I-43) and (I-44).

$$J_{yi}(\alpha_1,\beta) = \{ 0.5d\, e^{0.5j(2\ell-1)\pi} [J_o | 0.5(2\ell-1)\pi + \alpha_1 d | - e^{-j(2\ell-1)\pi} J_o | \alpha_1 d - 0.5(2\ell-1)\pi |] \} \{0.25w\pi\, e^{0.5j(k-1)\pi} [J_o | 0.5(k-1)\pi + 0.5\beta w | + e^{-j(2\ell-1)\pi} J_o | 0.5\beta w - 0.5(k-1)\pi |]\} \quad (I\text{-}43)$$

$$J_{zj}(\alpha_1,\beta) = \{ 0.5d\, e^{0.5j(2\ell-1)\pi} [J_o | 0.5(2\ell-1)\pi + \alpha_1 d | + e^{-j(2\ell-1)\pi} J_o | \alpha_1 d - 0.5(2\ell-1)\pi |] \} \{0.25w\pi\, e^{0.5j(k-1)\pi} [J_o | 0.5(k-1)\pi + 0.5\beta w | - e^{-j(2\ell-1)\pi} J_o | 0.5\beta w - 0.5(k-1)\pi |]\} \quad (I\text{-}44)$$

where J_o denodes the zero-order Bessel function of the first kind.

B. VALIDITY CHECK

To compare the present method with the experimental and computed data in the previous publication [7], we considered first special case $\varepsilon_1=\varepsilon_2=\varepsilon_3=1$. We assume that a dominant-mode incident electric field $E_{y10} = -j\beta_{10}\phi_1(x)e^{-j\beta_{10}z}$, where $\phi_1(x)$ is defined in Eq. (I-2), comes from the left of the waveguide. The numerical result has been checked by the power conservation law in which the equation $|R|^2 + |T|^2 = 1$ has to be satisfied, R and T are the reflection and transmission coefficients for the dominant-mode, and can be determined from C_{10}^- and C_{10}^+, which are given by Eq. (I-34). The calculated results for different

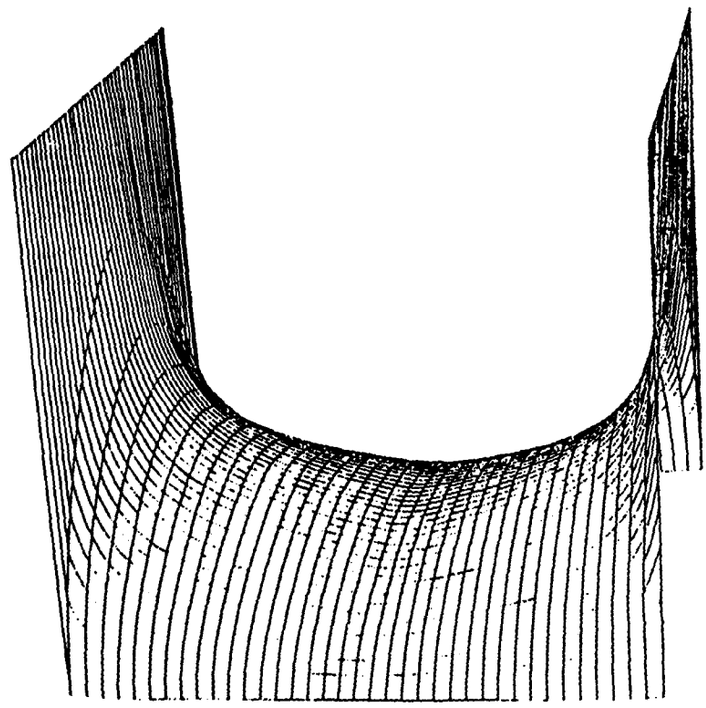

Fig. I-4 (a) Current distribution of basis function J_{y1}

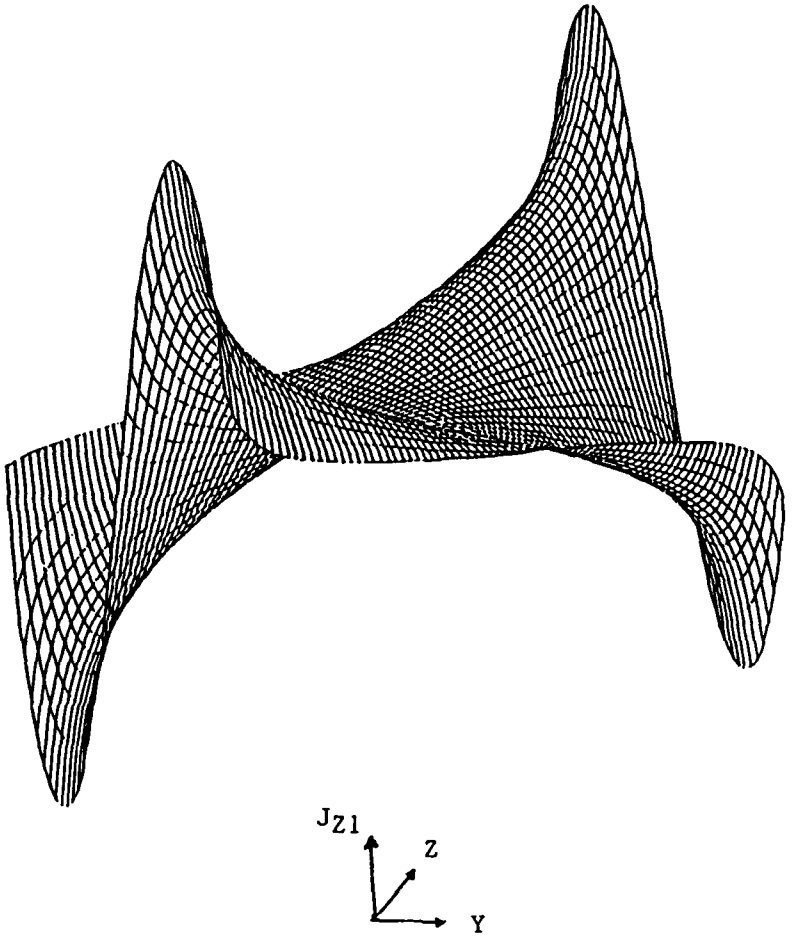

Fig. I-4 (b) Current distribution of basis function J_{z1}

Table 1: Confirmation of Power Conservation

$d_{(mm)}$	R		T		$\|R\|^2 + \|T\|^2$
0.5	-.02008	-.02598 j	.79080	-.61119 j	1.00000
1.0	-.14712	-.13549 j	.66376	-.72071 j	1.00000
1.5	-.70508	-.10766 j	.10580	-.69288 j	1.00000
2.0	-.78485	.61825 j	.02602	.03304 j	1.00000
2.5	-.53859	.77455 j	.27229	.18934 j	1.00000
3.0	-.45482	.79016 j	.35606	.20495 j	1.00000
3.5	-.38694	.79227 j	.42394	.20705 j	1.00000

$h_1 = h_3 = 3.43mm$, $h_2 = 0.254mm$, $\varepsilon_1 = \varepsilon_3 = 1$

$b = 3.56mm$ $w = 1.0m$ $f = 35GHz$ $\varepsilon_2 = 2.2$

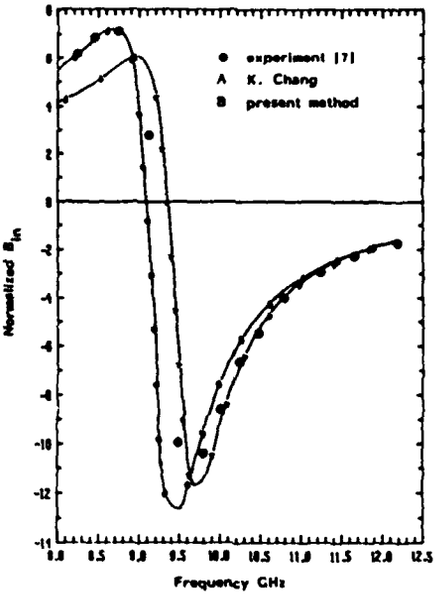

(a)

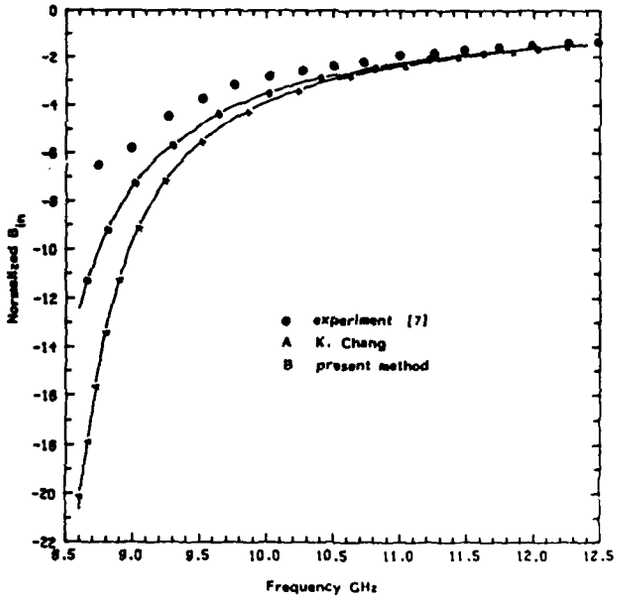

(b)

Fig. I-5 Normalized susceptance of an E-plane strip in an X-band waveguide for $\varepsilon_1=\varepsilon_2=\varepsilon_3=1$, a=22.86mm, b=10.16mm, (a) $h_1+h_2=12.57$mm, d=7.37mm, w=3.38mm. (b) $h_1+h_2=11.43$mm, d=9.19mm, w=1.7mm.

parameters are given in Table 1. It shows that $|R|^2 + |T|^2$ is essentially 1. The convergence test with different number of basis functions has been performed. Although accuracy can be increased with a larger number of basis functions, computation efforts also increase.

A comparison of the normalized susceptance versus frequency between the numerical results obtained by present approach and those given in [7] is shown in Fig. I-5(a) and (b). It is found that the numerical results agree well with the experimental data and Chang's data. It is believed that the present method is more accurate and can be improved systematically with the use of more basis functions.

C. RESULTS AND DISCUSSION

Figures I-6(a) and I-6(b) show the variations in normalized admittance versus frequency with different values of dielectric constant of the substrate in Region 2. As the dielectric constant of the substrate increases, the resonant frequency at which the B_{in} becomes zero decreases. This phenomenon happens because as the dielectric constant of the substrate increases the wavelengths corresponding to each mode become shorter. The resonant frequency and the characteristics of input admittance of the structure can be controlled by the dielectric constant of the substrate.

Figures I-7 and I-8 show the variations of normalized admittance versus the height and width of the strip at different frequencies for an E-plane fin inserted in a Ka-band rectangular waveguide. As shown in Fig. I-7, for a fixed width of the fin, the shorter the height , the higher the resonant frequency is, because the shorter

fin corresponds to smaller values of capacitance and inductance in the equivalent circuit. For a fixed height of the fin (Fig. I-8), the higher resonant frequency is related to a narrower fin, which has smaller capacitance. One way to obtain a given resonant frequency of this structure, is to change the dimension of the fin.

Figures I-9 and I-10 show the values of X_1 and X_2 versus the height d and the width w of the strip in an X-band rectangular waveguide. It is noted that for a given frequency, X_1 is not sensitive to d, whereas X_2 increases with d. When w increases, X_1 increases. On the other hand, X_2 decreases with w for a higher frequency and increases in a certain region of w for lower frequency. (Curve A in Fig. I-10(b)). Figures I-11 and I-12 are the data corresponding to those in Figs. I-9 and I-10 except that the frequencies are in the Ka-band. Figures I-13 and I-14 show X_1 and X_2 versus frequency with different values of height and width for the Ka-band waveguide. In Fig. I-13 it is seen that for a narrow strip X_1 varies slowly as frequency is increased, while X_2 varies faster for a narrower strip than for a wider one. Those informations are very useful from design point of view. For instance, to control the resonant frequency of this structure, it is much better to tune the height of the fin instead of changing its width. In this way, X_2 can be changed without affecting X_1 since only X_2 is sensitive to the variation of the height of the fin .

Figure I-15 shows the variation of normalized capacitance C and normalized inductance L versus d. It is noted that there are two regions. In one of

them (approximately corresponding to d=w, in this calculation w=1.0mm) C increases and L decreases as frequency increases. In another region C decreases and L increases as frequency becomes higher. It is conjectured that this phenomenon is related to the field distributions and to the use of the equivalent circuit chosen here.

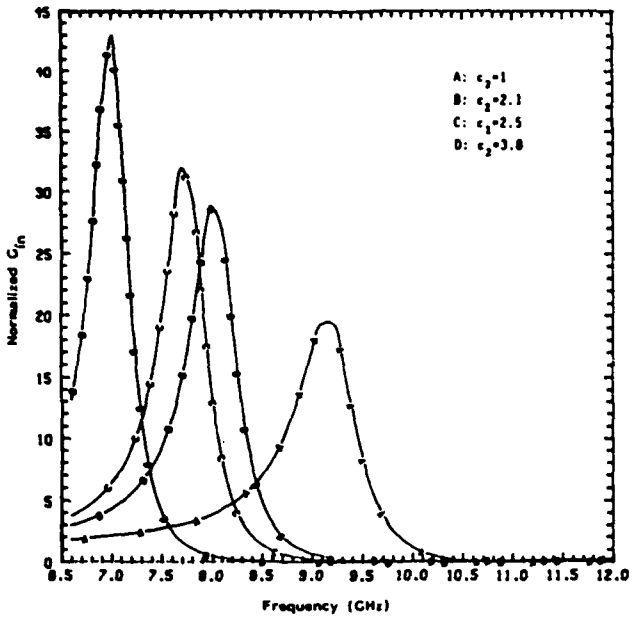

(a)

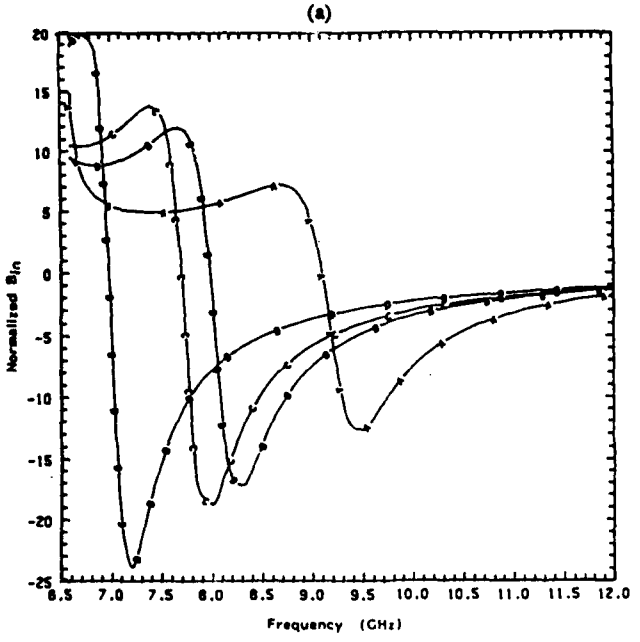

(b)

Fig. I-6 Normalized admittance of an E-plane strip in an X-band waveguide versus frequency for $\varepsilon_1 = \varepsilon_3 = 1$, $h_1 = 11.57$mm, $h_2 = 1.0$mm, d=7.37mm and w=3.38mm, (a) Normalized conductance versus frequency. (b) Normalized susceptance versus frequency.

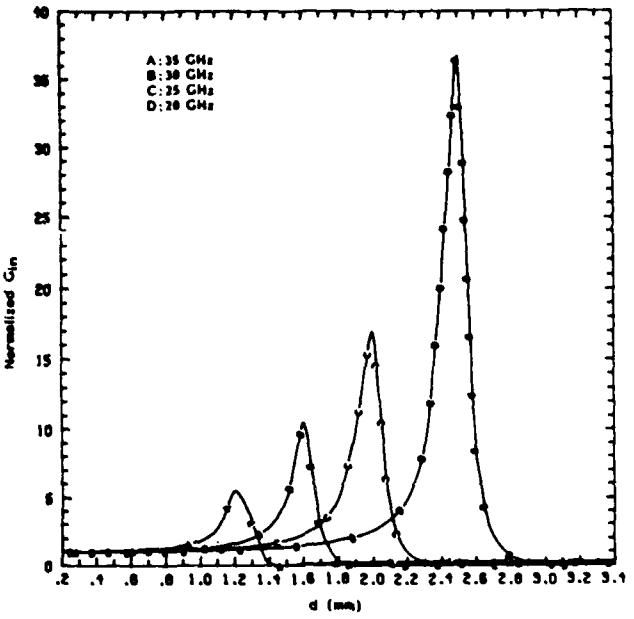

(a)

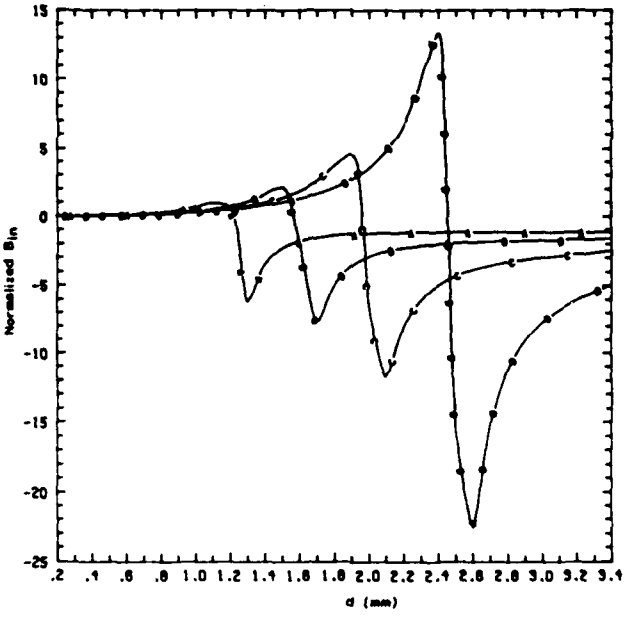

(b)

Fig. I-7 Normalized admittance of an E-plane strip in a Ka-band waveguide versus strip height for $\varepsilon_1=\varepsilon_3=1$, $\varepsilon_2=2.2$, $h_1=3.43$mm, $h_2=0.254$mm, a=7.11mm, b=3.56mm, w=1mm, (a) Normalized conductance versus strip height. (b) Normalized Susceptance versus strip height.

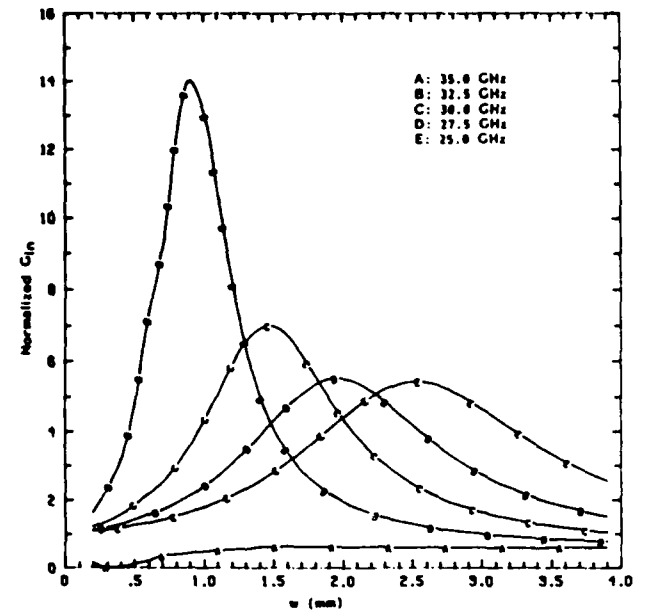

(a)

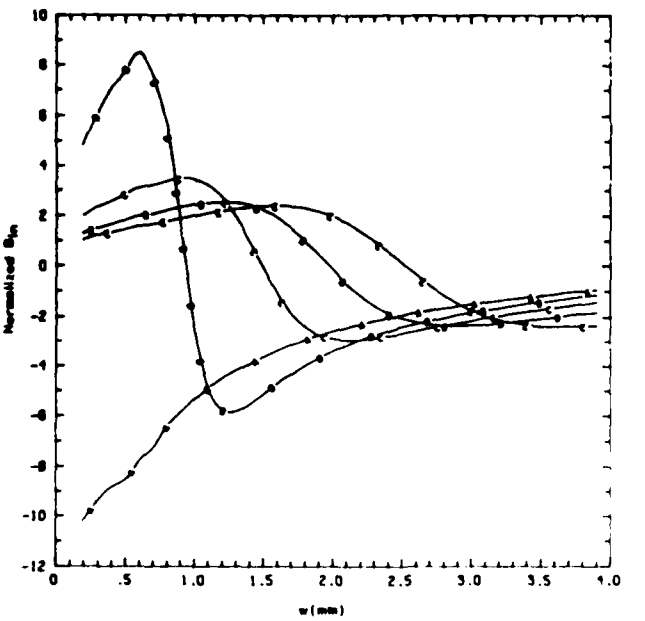

(b)

Fig. I-8 Normalized admittance of an E-plane strip in a Ka-band waveguide versus strip width for $\varepsilon_1=\varepsilon_3=1$, $\varepsilon_2=2.2$, $h_1=3.43$mm, $h_2=0.254$mm, d=1.78mm, (a) Normalized conductance versus strip width. (b) Normalized Susceptance versus strip width.

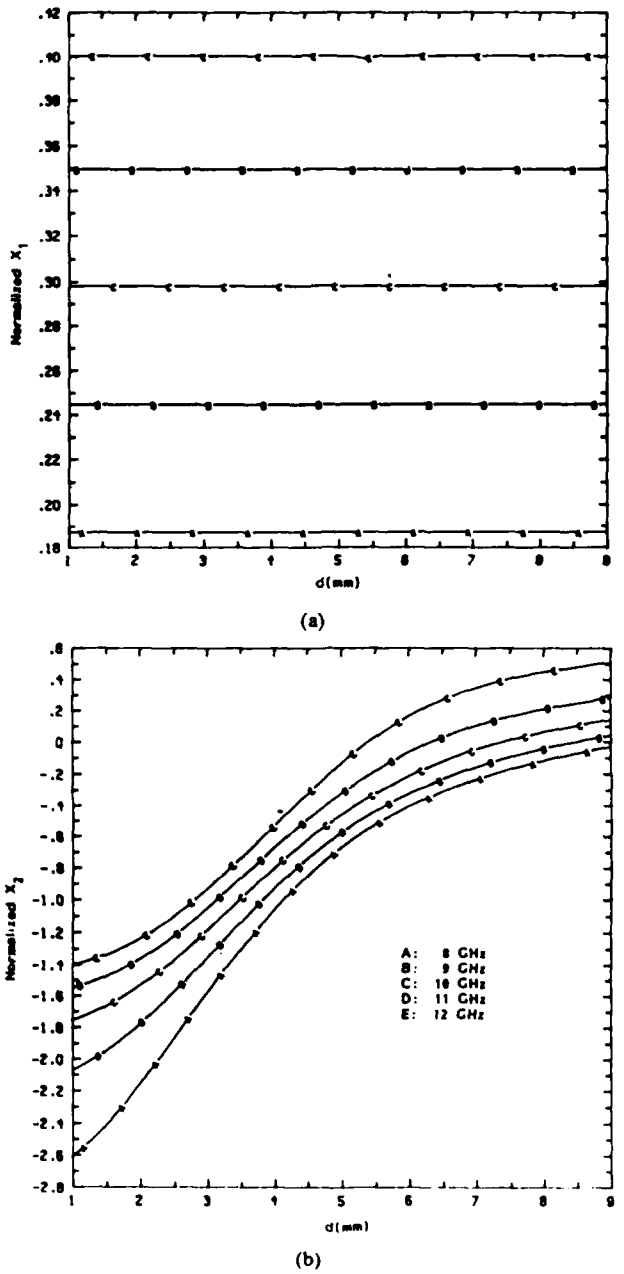

Fig. I-9 Normalized reactance of equivalent circuit of an E-plane strip in an X-band waveguide versus strip height for $\varepsilon_1=\varepsilon_3=1$, $\varepsilon_2=2.1$, $h_1=11.75$mm, $h_2=1.0$mm, w=3.38mm, (a) Normalized X_1 versus strip height. (b) Normalized X_2 versus strip height.

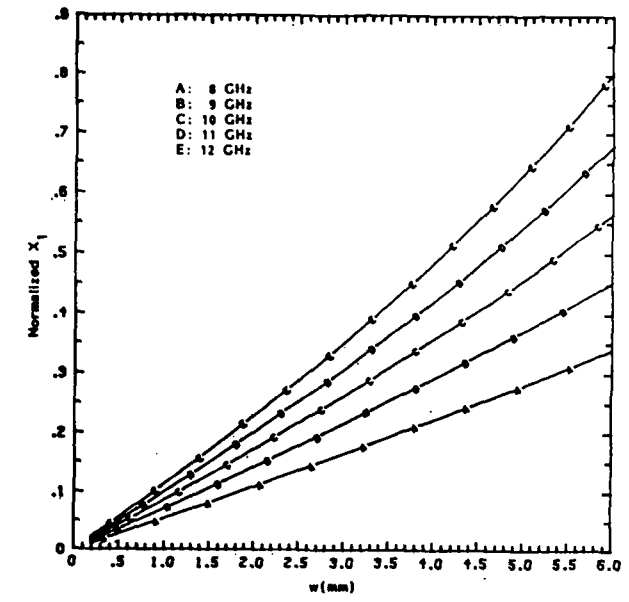

(a)

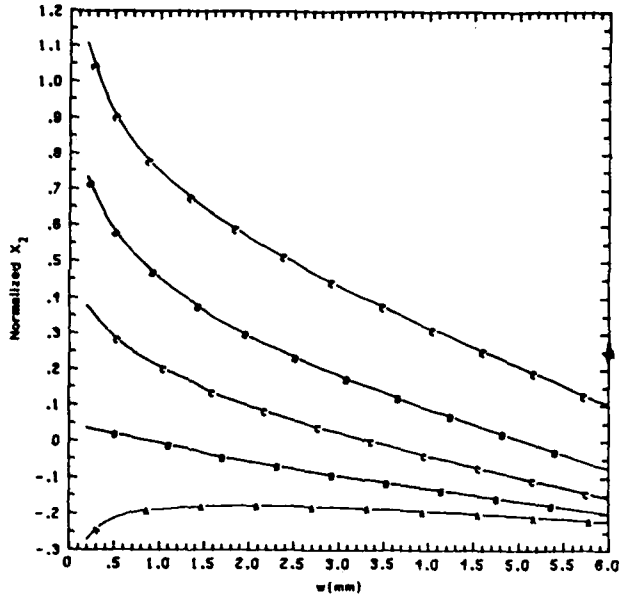

(b)

Fig. I-10 Normalized reactance of equivalent circuit of an E-plane strip in an X-band waveguide versus strip width $\varepsilon_1=\varepsilon_3=1$, $\varepsilon_2=2.1$, $h_1=11.75$mm, $h_2=1.0$mm, d=7.37mm, (a) Normalized X_1 versus strip width,(b) Normalized X_2 versus strip width

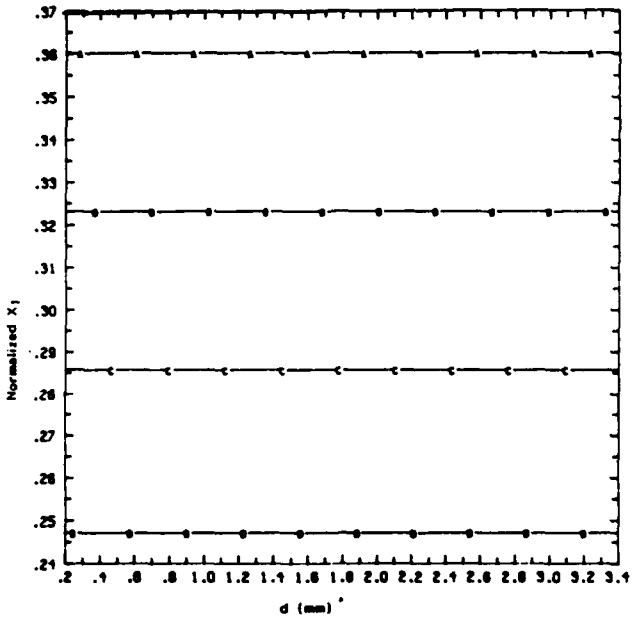

(a)

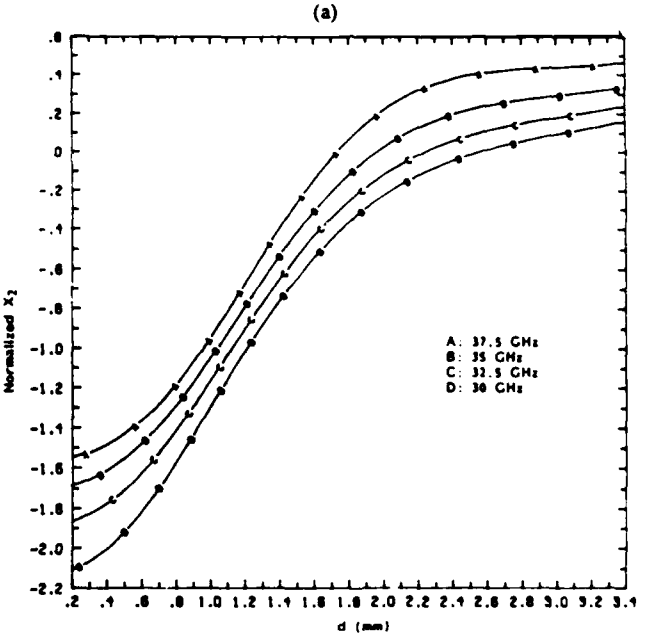

(b)

Fig. I-11 Normalized reactance of equivalent circuit of an E-plane strip in a Ka-band waveguide versus strip height for $\varepsilon_1=\varepsilon_3=1$, $\varepsilon_2=2.2$, $h_1=3.43$mm, $h_2=0.254$mm, w=1mm, (a) Normalized X_1 versus strip height. (b) Normalized X_2 versus strip height.

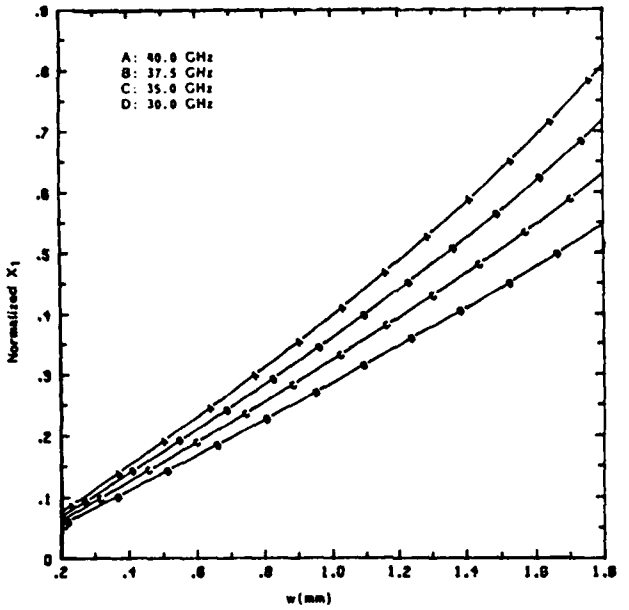

(a)

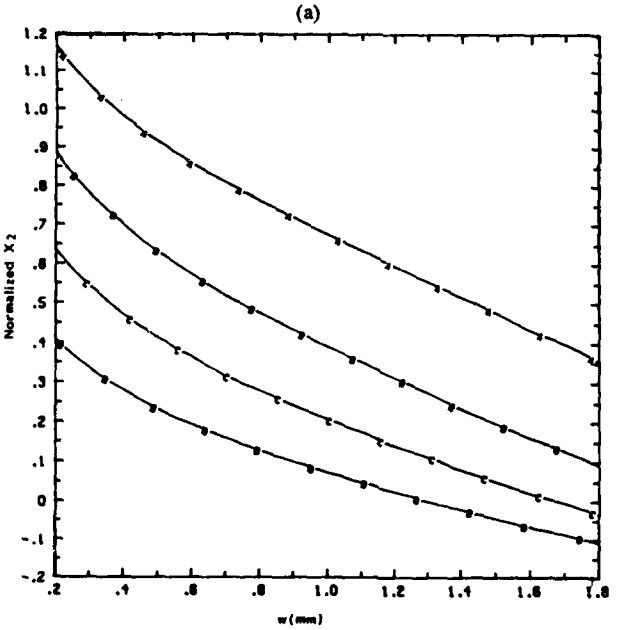

(b)

Fig. I-12 Normalized reactance of equivalent circuit of an E-plane strip in a Ka-band waveguide versus strip width for $\varepsilon_1=\varepsilon_3=1$, $\varepsilon_2=2.2$, $h_1=3.43$mm, $h_2=0.254$mm, d=2.45, (a) Normalized X_1 versus strip width. (b) Normalized X_2 versus strip width.

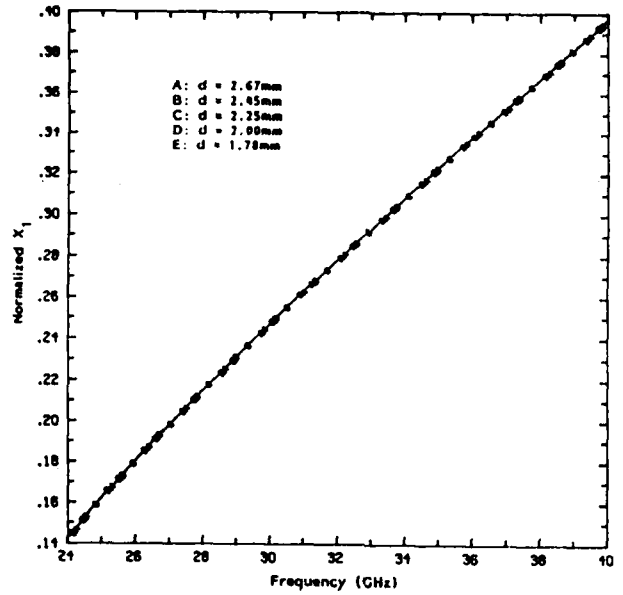

(a)

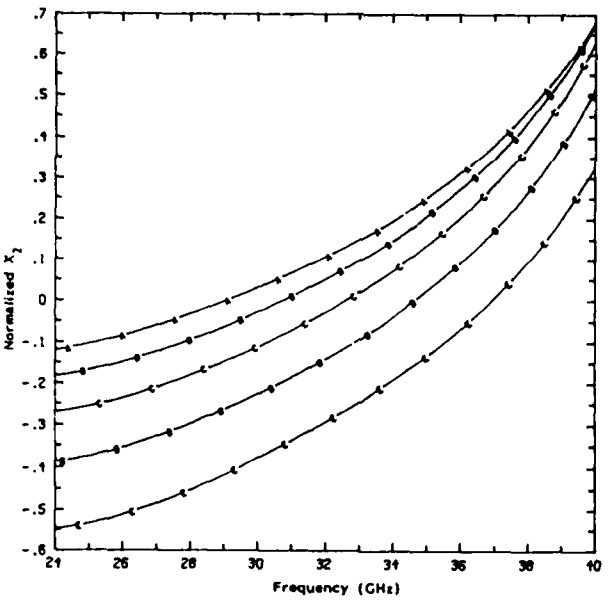

(b)

Fig. I-13 Normalized reactance of equivalent circuit of an E-plane strip in a Ka-band waveguide versus frequency for different strip height $\varepsilon_1=\varepsilon_3=1$, $\varepsilon_2=2.2$, $h_1=3.43$mm, $h_2=0.254$mm, w=1mm, (a) Normalized X_1 versus frequency(b) Normalized X_2 versus frequency.

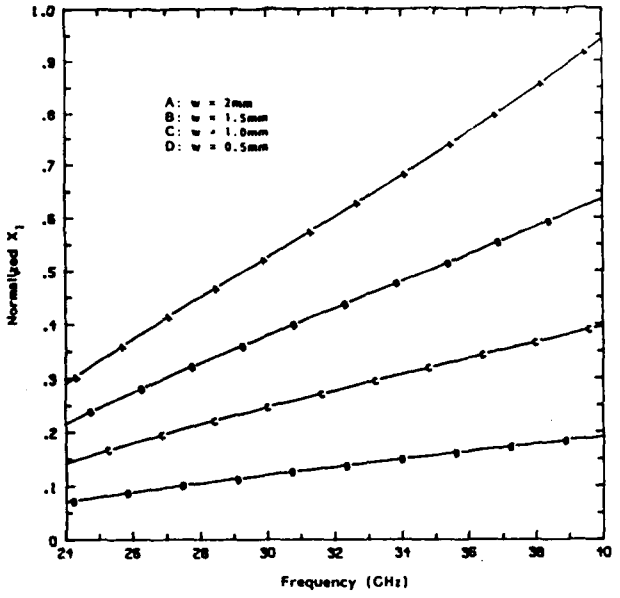

(a)

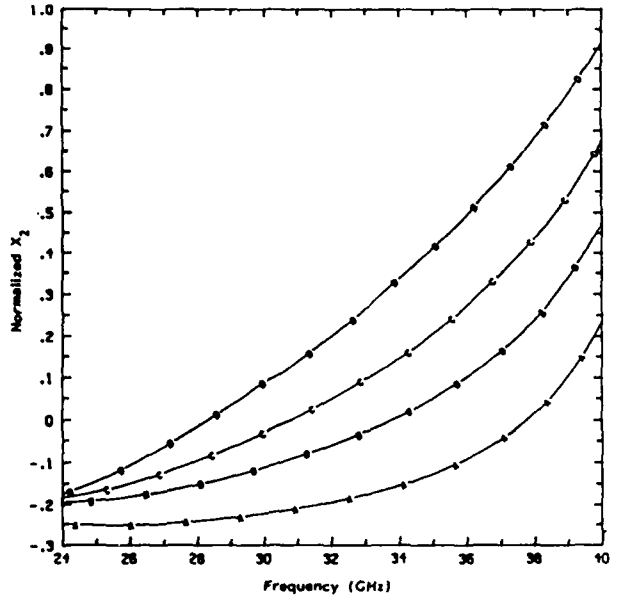

(b)

Fig. I-14 Normalized reactances of equivalent circuit of an E-plane strip in a Ka-band waveguide versus frequency for different strip width $\varepsilon_1=\varepsilon_3=1$, $\varepsilon_2=2.2$, $h_1=3.43$mm, $h_2=0.254$mm, d=2.45mm, (a) Normalized X_1 versusfrequency(b) Normalized X_2 versus frequency.

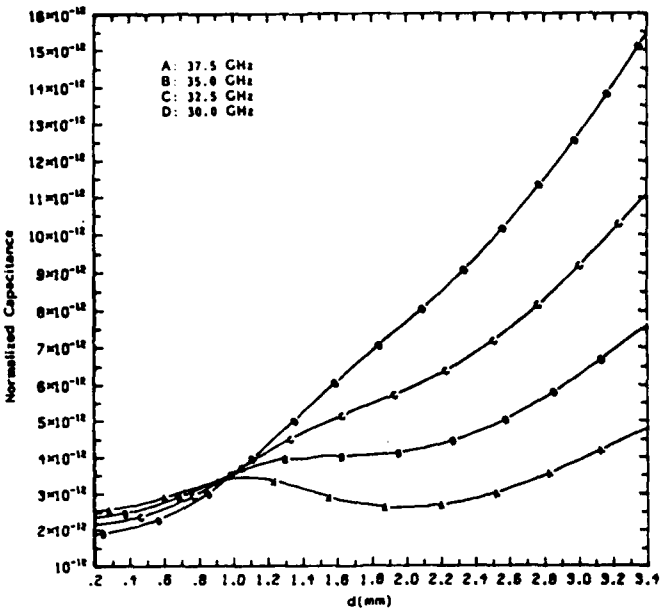

(a)

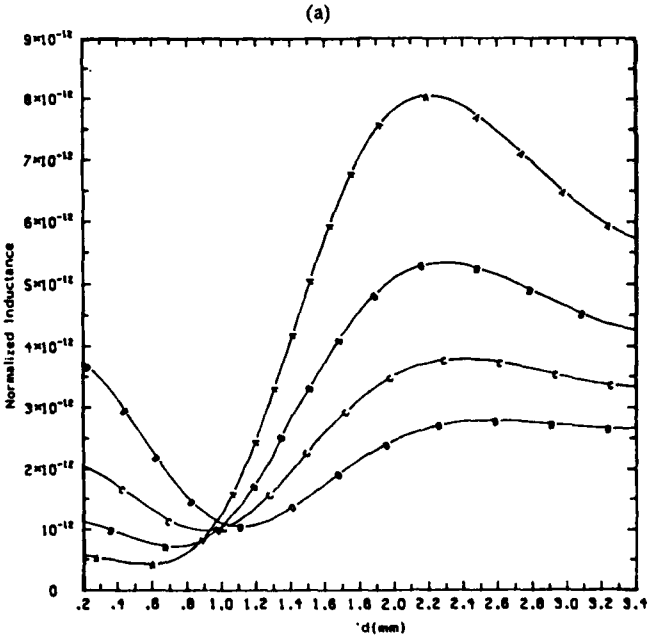

(b)

Fig. I-15 Normalized equivalent circuit element values C and L of a narrow E-plane strip as a function of the strip height. $\varepsilon_1=\varepsilon_3=1$, $\varepsilon_2=2.2$, $h_1=3.43$mm, $h_2=0.254$mm, w=1mm, (a) Normalized C versus strip height. (b) Normalized L versus strip height.

IV CONCLUSIONS

A new analytical technique has been developed, that can be used for characterizations of the scattering phenomena of planar E-plane obstacles. The numerical results for a special case agree well with experimental and published data. The curves of normalized input admittance and equivalent circuit element values are presented for a number of different parameters of this structure. This technique is believed to bo useful in the design of microwave filters and other planar circuit components.

PART TWO

ANALYSIS AND DESIGN OF EVANESCENT MODE WAVEGUIDE BANDPASS FILTER WITH NON-TOUCHING E-PLANE FINS

I INTRODUCTION

In the late 1950's Jaynes [1] and Edson [2] proposed that resonators built in cutoff waveguide may be used in filter design. These kinds of filters are called evanescent mode (or 'ghost mode' as Jaynes called it) filters. Microwave bandpass filters using evanescent modes have been designed successfully [3,4,5]. The evanescent mode bandpass filter has several advantages compared to the conventional type of bandpass filters (waveguide above cutoff, coaxial line etc.). For instance, a sharper transition to out-of-band rejection can be obtained on the higher frequency side. Evanescent mode waveguide filters are also smaller than traditional waveguide filters. A waveguide operating below its cutoff frequency is basically an inductive element [5,6]. Suitable capacitive elements are needed to construct an evanescent mode waveguide bandpass filter. Evanescent mode filters using conventional capacitive elements such as tuning screws [4,5] are costly and difficult to mass produce because of their complicated structure. Non-touching E-plane fins[7], which are easily to fabricated, are proposed in this study as the capacitive elements. The filter structure, shown in Fig. II-1, consists of a number of non-touching E-plane fins placed in a rectangular waveguide below cutoff. The fins may be metal only or supported by a dielectric layer. The input and output portions of the filter are coupled to the external circuits via double step waveguide junctions. The larger waveguides operate above the cutoff frequency. Since the capacitive elements utilize a printed circuit structure, they are suitable for mass production at low cost.

The initial approach to the synthesis of an evanescent mode filter was based on image-parameter theory [3]. This approach cannot be used for exact design

technique to obtain the scattering matrix description of the evanescent mode filter. The insertion loss and the return loss of the filter then can be obtained from the final scattering matrix.

Filters designed with the present technique have been tested in Ka band (26.5-40.0 GHz). Good agreement between theory and measurement is observed.

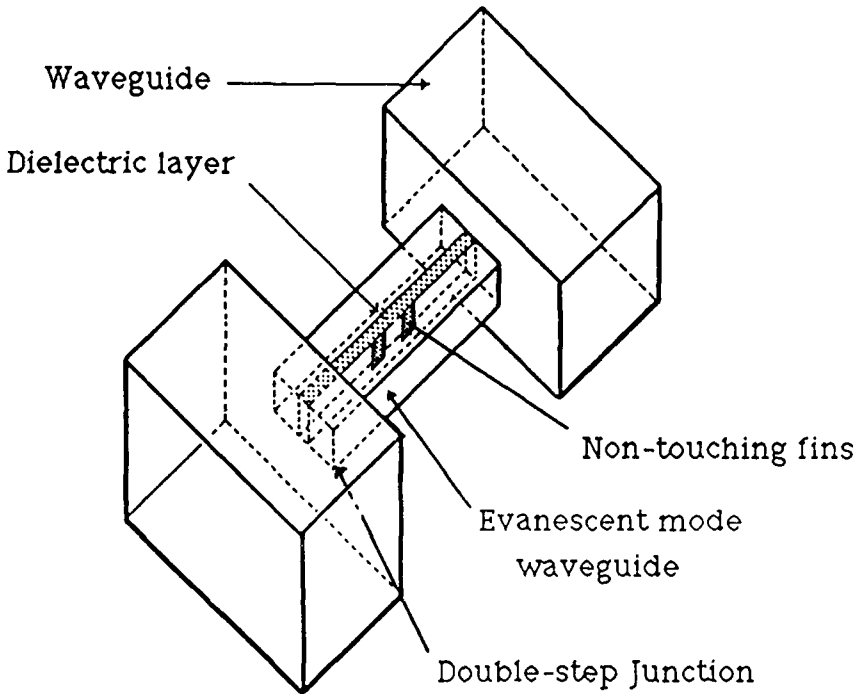

Fig. II-1 The structure of evanescent mode wavaguide Filter with non-touching E-plane fins.

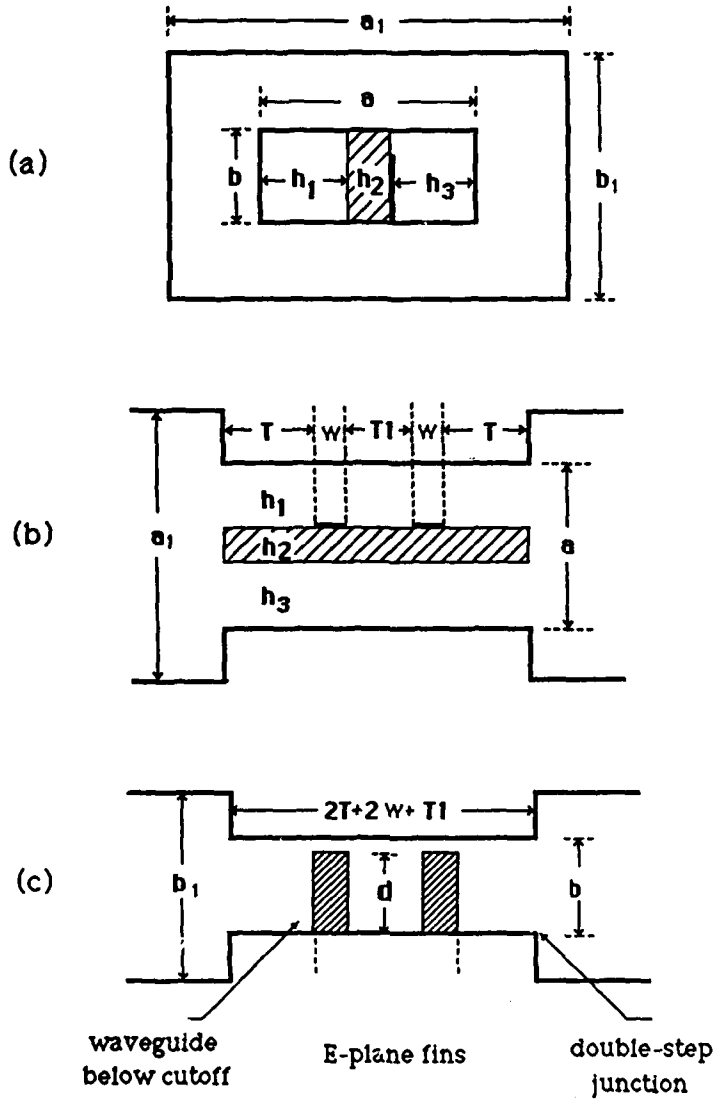

Fig. II-2 (a) Cross sectional view; (b) Top view; (c) Side view of the filter.

II. ANALYSIS AND DESIGN PROCEDURE

The analysis and design of an evanescent mode waveguide bandpass filter with non-touching E-plane fin is based on the generalized scattering matrix technique in conjunction with the spectral domain approach and the mode matching method. The study begin with brief description of the generalized scattering matrix . Then the scattering matrix representations for the double-step junction, the non-touching E-plane fins, and the evanescent mode waveguide section are obtained by the mode matching technique, spectral domain method, and waveguide theory, respectively. Finally, these scattering matrices are combined to obtain the final generalized scattering matrix. The filter response is calculated from the final scattering matrix.

A . GENERALIZED SCATTERING MATRIX

The concept of a generalized scattering matrix, introduced by Mittra and Pace [10], is closely related to the scattering matrix of circuit theory or of microwave network theory. It differs by including scattering of all modes, so that the scattering matrix will in general be of infinite order. In the following discussion, the term " scattering matrix " will mean "generalized scattering matrix ."

The scattering matrix can be defined for a junction discontinuity at which the fields may be expanded in modes, such as the double-step waveguide junction show in Fig.II-3. Consider that the *mn*th TE mode is incident upon the plane z=0 from the larger waveguide I and waves are reflected back into waveguide I and transmitted into smaller waveguide II. If the amplitude of the *mn*h TE incident in I is normalized

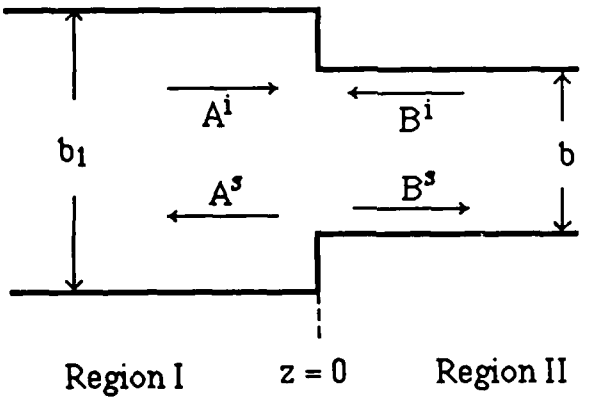

$$\begin{bmatrix} A^s \\ B^s \end{bmatrix} = \begin{bmatrix} \mathbf{S} \end{bmatrix} \begin{bmatrix} A^i \\ B^i \end{bmatrix}$$

Fig. II-3 Side view of double-step waveguide junction.

to unity, then the amplitude of the *pq*th TE scattered mode in waveguide I is $S^{EE}_{I\,I}$ (pq,mn), and the amplitude of the *pq*th transmitted TM mode in waveguide II is $S^{ME}_{II\,I}$ (pq,mn) . The terms $S^{ME}_{II\,I}$ (pq,mn) and $S^{EE}_{I\,I}$ (pq,mn) are the generalized matrix elements of $S^{ME}_{II\,I}$ and $S^{EE}_{I\,I}$, respectively. The other scattering matrixes , such as $S^{EM}_{I\,II}$, $S^{EE}_{II\,I}$, and $S^{MM}_{II\,I}$, etc., may be similarly defined [10,11]. In conventional scattering matrix formulations, the propagating modes are normalized so that a mode carries unit power. Since the generalized scattering matrix includes evanescent modes, such a normalization is inappropriate. One consequence is that the scattering matrix is not symmetric.

In the notation used above, the scattering matrix relates the excited modes to the incident ones via :

$$\begin{pmatrix} A^s \\ B^s \end{pmatrix} = [S] \begin{pmatrix} A^i \\ B^i \end{pmatrix} = \begin{pmatrix} S_{I\,I} & S_{I\,II} \\ S_{II\,I} & S_{II\,II} \end{pmatrix} \begin{pmatrix} A^i \\ B^i \end{pmatrix} \qquad (\text{II-1})$$

The superscript s indicates scattered fields, and i expresses the incident fields. The general element of **S** is $S^{xy}_{i\,j}$ (pq,mn), where x and y = E or M, represent a TE or TM to **x** wave; i and j = I or II indicate the Region I or Region II; m, n, p and q are integers corresponding to different modes. For example, $S^{ME}_{II\,I}$(11,10) repressents the ratio of the amplitude of reflected TM_{11} in Region II to the amplitude of an incident TE_{10} wave in Region I. In more detail the above equation runs as follows:

$$
\begin{bmatrix}
A_E^s(10) \\ A_E^s(20) \\ \vdots \\ A_M^s(01) \\ A_M^s(02) \\ \vdots \\ B_E^s(10) \\ B_E^s(20) \\ \vdots \\ B_M^s(01) \\ B_M^s(02) \\ \vdots
\end{bmatrix}
=
\begin{bmatrix}
S_{I\,I}^{EE}(10,10) & S_{I\,I}^{EE}(10,20) & \cdots & S_{I\,II}^{EM}(10,01) & S_{I\,II}^{EM}(10,02) \cdots \\
S_{I\,I}^{EE}(20,10) & S_{I\,I}^{EE}(20,20) & \cdots & S_{I\,II}^{EM}(20,01) & S_{I\,II}^{EM}(20,02) \cdots \\
\vdots & \vdots & & \vdots & \vdots \\
S_{I\,I}^{ME}(01,10) & S_{I\,I}^{ME}(01,20) & \cdots & S_{I\,II}^{MM}(01,01) & S_{I\,II}^{MM}(01,02) \cdots \\
S_{I\,I}^{ME}(02,10) & S_{I\,I}^{ME}(02,20) & \cdots & S_{I\,II}^{MM}(02,01) & S_{I\,II}^{MM}(02,02) \cdots \\
\vdots & \vdots & & \vdots & \vdots \\
S_{II\,I}^{EE}(10,10) & S_{II\,I}^{EE}(10,20) & \cdots & S_{II\,II}^{EM}(10,01) & S_{II\,II}^{EM}(10,02) \cdots \\
S_{II\,I}^{EE}(20,10) & S_{II\,I}^{EE}(20,20) & \cdots & S_{II\,II}^{EM}(20,01) & S_{II\,II}^{EM}(20,02) \cdots \\
\vdots & \vdots & & \vdots & \vdots \\
S_{II\,I}^{ME}(01,10) & S_{II\,I}^{ME}(01,20) & \cdots & S_{II\,II}^{MM}(01,01) & S_{II\,II}^{MM}(01,02) \cdots \\
S_{II\,I}^{ME}(02,10) & S_{II\,I}^{ME}(02,20) & \cdots & S_{II\,II}^{MM}(02,01) & S_{II\,II}^{MM}(02,02) \cdots \\
\vdots & \vdots & & \vdots & \vdots
\end{bmatrix}
\begin{bmatrix}
A_E^i(10) \\ A_E^i(20) \\ \vdots \\ A_M^i(01) \\ A_M^i(02) \\ \vdots \\ B_E^i(10) \\ B_E^i(20) \\ \vdots \\ B_M^i(01) \\ B_M^i(02) \\ \vdots
\end{bmatrix}
\qquad \text{(II-2)}
$$

Theoretically the generalized matrix is of infinite dimensions corresponding to the infinite number of eigenmodes. The matrix is truncated to finite size for numerical calculations.

The generalized scattering matrix technique is useful for dealing with structures containing several discontinuities. For example, the structure of evanescent mode waveguide filter with non-touching fins consists of three portions: the double-step waveguide junctions and the non-touching E-plane fin portion, and the waveguide below cutoff. Each portion of the structure can be represented by its

corresponding scattering matrix. These matrices are then combined to obtain the scattering matrix of the filter structure. The insertion loss and the return loss can be obtained from the related elements of final scattering matrix.

B. SCATTERING MATRIX REPRESENTATION OF A DOUBLE-STEP JUNCTION

In this section the scattering matrix representation of a double-step junction is derived via the mode matching technique[12,13]. As shown in Fig. II-3 Region I represents the larger guide and the smaller guide is denoted by Region II. The field is derived from the electric vector potential **F** and the magnetic vector potential **A** [14].

$$\mathbf{E} = -\nabla \times \mathbf{F} + \nabla \times \nabla \times \mathbf{A} / j\omega\varepsilon_0 \qquad (II\text{-}3)$$

$$\mathbf{H} = \nabla \times \mathbf{A} + \nabla \times \nabla \times \mathbf{F} / j\,\omega\mu_0 \qquad (II\text{-}4)$$

In this study, it is convenient to choose

$$\mathbf{A} = \psi \mathbf{x} \qquad (II\text{-}5)$$

$$\mathbf{F} = \phi \mathbf{x} \qquad (II\text{-}6)$$

where ψ and ϕ are the scalar functions which represent the electric (TE) wave and magnetic (TM) wave transverse to the x-direction, respectively, and **x** is a unit vector in the x-direction. These potentials are extended in terms of their eigenfunctions which must satisfy the boundary conditions. The potentials in each

region can be expressed as follows:

$$\phi_i = \sum_{m=1}^{M} \sum_{n=0}^{N-1} [\, a_{imn} \exp(-k_{izhmn} z) + b_{imn} \exp(k_{izhmn} z)] P_{imn}(x,y) \qquad (\text{II-7})$$

$$\psi_i = \sum_{m=0}^{M-1} \sum_{n=1}^{N} [\, c_{imn} \exp(-k_{izemn} z) + d_{imn} \exp(k_{izemn} z)] Q_{imn}(x,y) \qquad (\text{II-8})$$

(The notation used in this part is described below:

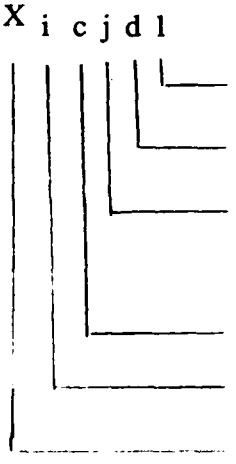

l = *m*, *n* or *mn* indicates *m*th, *n*th or *mn*th mode

d = h or e, h : TE-to-x field ; e : TM - to -x field

j = 1, 2, or 3 indicates the variable in the region 1, 2, or 3 of the smaller waveguide.

c = x, y, or z indicated the x- , y- or z-direction, respectively

i = I or II, I : larger waveguide; II : smaller waveguide

indicate the variable)

where

$$P_{imn}(x,y) = R_{im}(x) S_{in}(y) \qquad (\text{II-9})$$

$$Q_{imn}(x,y) = T_{im}(x) V_{in}(y) \qquad (\text{II-10})$$

are the eigenfunctions of the TE-to -x and TM-to-x field, respectively. In region I, these eigenfunctions are represented by :

$$R_{Im}(x) = N_{rIm} \sin (m\pi x / a_1) \qquad (II\text{-}11)$$

$$S_{In}(y) = N_{sIn} \cos(n\pi y / b_1) \qquad (II\text{-}12)$$

$$N_{rIm} = \sqrt{(\delta_{mo} - 1) / a_1} \qquad N_{sIn} = \sqrt{(\delta_{no} + 1) / b} \qquad (II\text{-}13)$$

$m = 1, 2, 3, \cdots M \qquad n = 0, 1, 2, \cdots N-1$

$$T_{Im}(x) = N_{tIm} \cos (m\pi x / a_1) \qquad (II\text{-}14)$$

$$V_{In}(y) = N_{vIn} \sin (n\pi y / b_1) \qquad (II\text{-}15)$$

$$N_{tIm} = \sqrt{(\delta_{mo} + 1) / a_1} \qquad N_{vIn} = \sqrt{(\delta_{no} - 1) / a_1} \qquad (II\text{-}16)$$

$m = 0, 1, 2, \cdots M-1 \qquad n = 1, 2, 3, \cdots N$

where δ_{mo} and δ_{no} are the Kronecker delta functions. In Region II, the eigenfunctions are given by :

$$S_{IIq}(y) = N_{sIIq} \cos[(q\pi / b_1)(y-y_1)] \qquad (II\text{-}17)$$

$$N_{sIIq} = \sqrt{(\delta_{qo} + 1) / b_1} \qquad (II\text{-}18)$$

$$R_{IIp}(x) = \begin{cases} N_{rII1p} \sin k_{IIx1hp}(x - x_1) & x_1 < x < x_1 + h_1 \\ N_{rII2p} \sin k_{IIx2hp}(x-x_1-h_1) & \\ \quad + N_{rIImp} \cos k_{rII2hp}(x-x_1-h_1) & x_1 + h_1 < x < x_1 + h_1 + h_2 \\ N_{rII3p} \sin k_{IIx3hp}(x-x-a) & x_1 + h_1 + h_2 < x < x_1 + a \end{cases} \qquad (II\text{-}19)$$

$p = 1, 1, 2, \cdots P \qquad q = 0, 1, 2, \cdots Q-1$

$$V_{IIq}(y) = N_{vIIq} \sin [(q\pi / b_1)(y-y_1)] \qquad (II\text{-}20)$$

$$N_{vIIq} = \sqrt{(\delta_{no} - 1) / a_1} \qquad (II\text{-}21)$$

$$T_{IIp}(x) = \begin{cases} N_{tII1p} \cos k_{IIx1ep}(x-x_1) & x_1 < x < x_1 + h_1 \\ N_{tII2p} \cos k_{IIx2ep}(x-x_1-h_1) & \\ + N_{tIIp} \sin k_{IIx2ep}(x-x_1-h_1) & x_1 + h_1 < x < x_1 + h_1 + h_2 \\ N_{tII3p} \sin k_{IIx3ep}(x-x_1-a) & x_1 + h_1 + h_2 < x < x_1 + a \end{cases} \qquad (II\text{-}22)$$

$p = 0, 1, 2, \cdots P-1 \qquad q = 1, 2, 3, \cdots Q$

where N_{rIIj} and N_{tIIj}, j = 1, 2, and 3, are normalized coefficients of eigenfunctions $R_{IIm}(x)$ and $T_{IIm}(x)$ of the smaller waveguide in region j, respectively. They are given in Appendix C. The *m*th eigenmodes of TE-to-x and TM-to-x fields in the partially filled waveguide in region j are represented by k_{IIxjhm} and k_{IIxjem} (They correspond to γ_{im} and γ'_{im} in Part one of this study and can be found as described in Part one). Here k_{izhmn} and k_{izemn} are the propagation constants of the *mn* th TE- and TM-to-x fields in the z-direction, and must satisfy the following dispersion equations

$$k^2_{Izdmn} + k_o^2 = (m\pi / a_1)^2 + (n\pi / b_1)^2 \qquad (II\text{-}23)$$

$$k^2_{IIzdmn} + k_j^2 = k^2_{IIxjdm} + (n\pi / b)^2 \qquad (II\text{-}24)$$

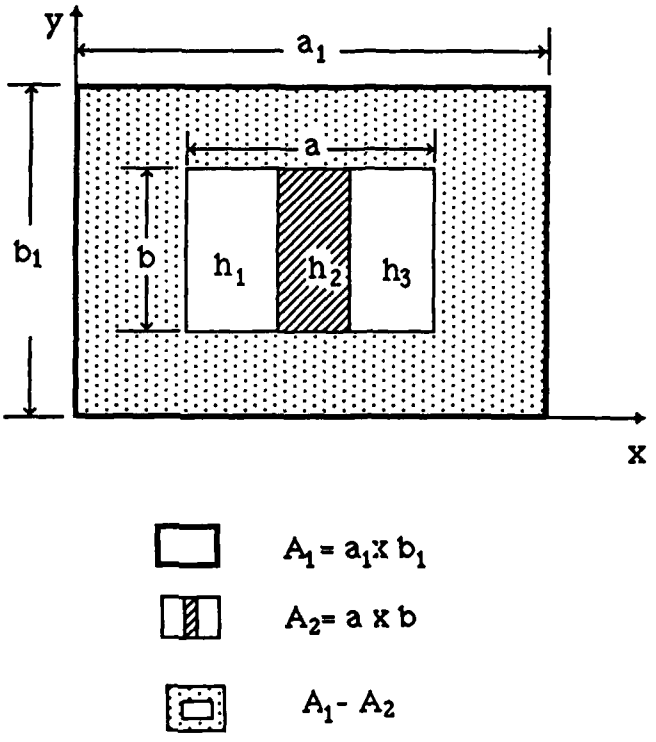

Fig. II-4 Cross sectional view (at z =0) of double-step waveguide junction

where d = h or e, j = 1, 2, and 3, k_o is the wave number in free space, $k_j = \sqrt{\varepsilon_j} k_o$, and ε_j is the relative dielectric constant of the smaller guide in region j. The coefficients a_{imn}, b_{imn}, c_{imn}, and d_{imn} in Eqs. (II-7) and (II-8) correspond to incident and reflected waves and are related to each other by the scattering matrix. The scattering matrix can be determined by matching the tangential fields at the step discontinuity at z = 0. (Fig. II-4)

$$E_{Ix,y} \text{ l at } z=o = E_{IIx,y} \text{ l at } z=o \qquad \text{in area } A_2$$

$$H_{Ix,y} \text{ l at } z=o = H_{IIx,y} \text{ lat } z=o \qquad \text{in area } A_2$$

$$E_{Ix,y} \text{ l at } z=o = 0 \qquad \text{in area } A_1 - A_2 \qquad \text{(II-25)}$$

Applying the orthogonality relationship between potential functions leads to the matrix equation :

$$\underbrace{\begin{pmatrix} Ma_I & 0 & -V_{bII} & 0 \\ 0 & V_{cI} & 0 & -M_{dII} \\ M_{bI} & M_{cI} & -V_{aII} & V_{dII} \\ V_{aI} & -V_{dI} & M_{bII} & M_{cII} \end{pmatrix}}_{M_1} \begin{pmatrix} A_{Imn} \\ C_{Imn} \\ B_{IIpq} \\ D_{IIpq} \end{pmatrix} = \underbrace{\begin{pmatrix} -M_{aI} & 0 & V_{bII} & 0 \\ 0 & -V_{cI} & 0 & M_{dII} \\ -M_{bI} & M_{cI} & V_{aII} & V_{dII} \\ V_{aI} & V_{dI} & M_{bII} & -M_{cII} \end{pmatrix}}_{M_2} \begin{pmatrix} B_{Imn} \\ D_{Imn} \\ A_{IIpq} \\ C_{IIpq} \end{pmatrix}$$

where M_{aI}, M_{cI}...ect. express matrices. For instance, M_{aI} is a matrix of dimensions PQ x MN. V_{bII}, V_{aI} ... are diagonal matrix of dimensions PQ x PQ, MN x MN ...,

A_{mn}, D_{pq}...ect. are vectors of dimensions MN or PQ, and are given in Appendix D.

The scattering matrix of the double-step discontinuity is then given by

$$S_d = \begin{bmatrix} S_{d11} & S_{d12} \\ S_{d21} & S_{d22} \end{bmatrix} = M_2^{-1} \cdot M_1 \qquad \text{(II-26)}$$

To check the validity of the calculations, we calculated the scattering parameters of a double-step waveguide discontinuity from Ku to K band (15.8 x 7.9 mm^2 to 10.7 x 4.32 mm^2) and compared results with Arndt and Wriedt 's[15]. The results are shown in Fig. II-5. They are in good agreement . Also, the magnitudes of the scattering parameters of resonant irises with finite thickness t (Fig. II-6) are obtained by combining two step junctions with a evanescent mode waveguide of length of t. The numerical results are compared with available data [12] and are shown in Fig.II-7 and Fig. II-8. Once again close agreement is observed.

C. SCATTERING MATRIX REPRESENTATION FOR THE PORTION OF NON-TOUCHING FINS

The scattering matrix for a non-touching fin can be obtained by combining the spectral domain method with residue calculus. (The details are described in the first part of the dissertation.) Since the filter may contain more then one fin element, a general case must be considered here. Figure II-9 shows that a structure consists of n fins , which are indicated by F_1, F_2, ... and F_n. These fins are separated from one to another by distances T_1, T_2,... and T_{n-1}. To obtain a scattering matrix representation S_f for this portion, we consider that a substructure which consists of

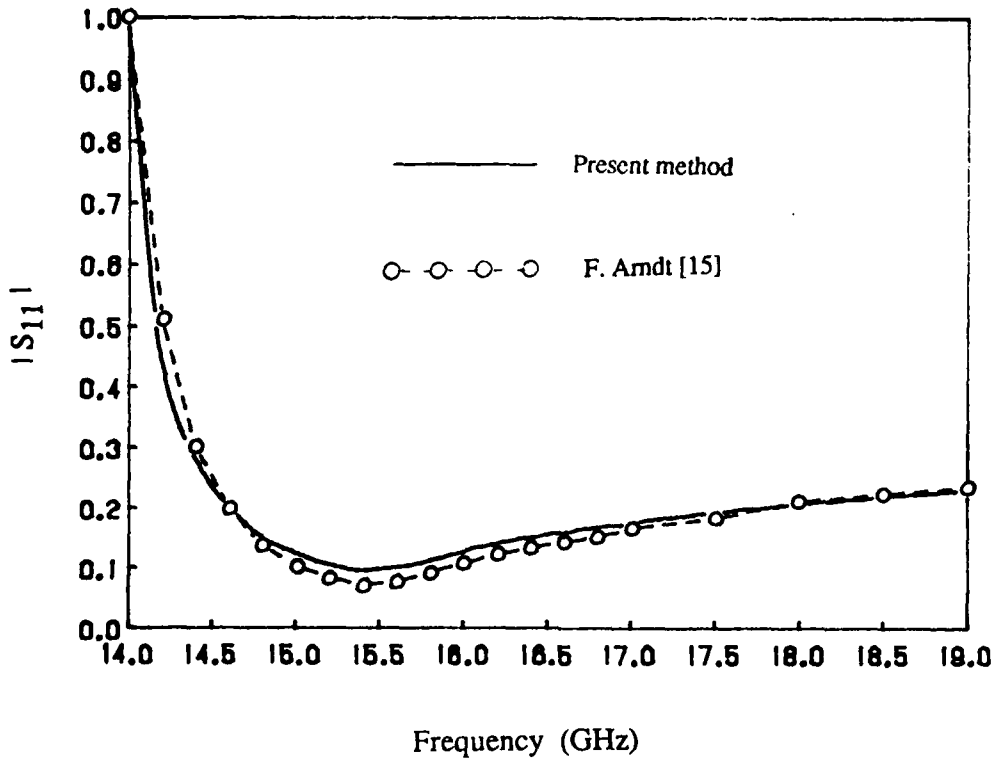

Fig. II-5 Reflection coefficient $|S_{11}|$ as a function of frequency, if a TE_{10} wave is incident from Ku-band waveguide (15.8 x 7.9 mm^2) to K-band guide (10.7 x 4.32 mm^2)

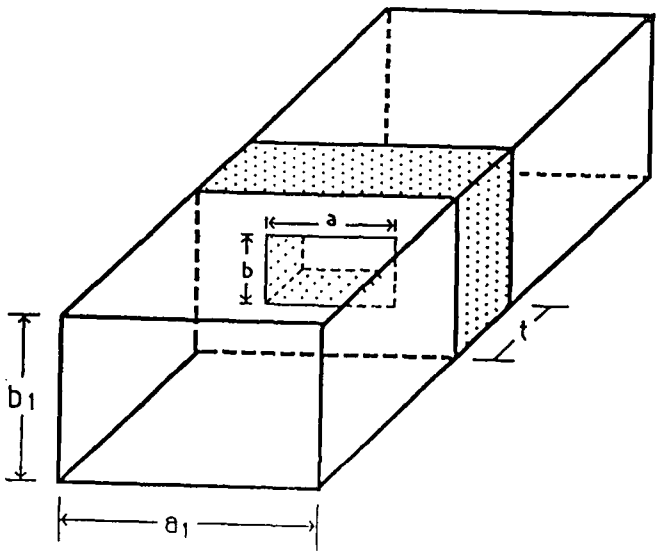

Fig. II-6 Resonant iris with finite thickness t in a rectangular waveguide.

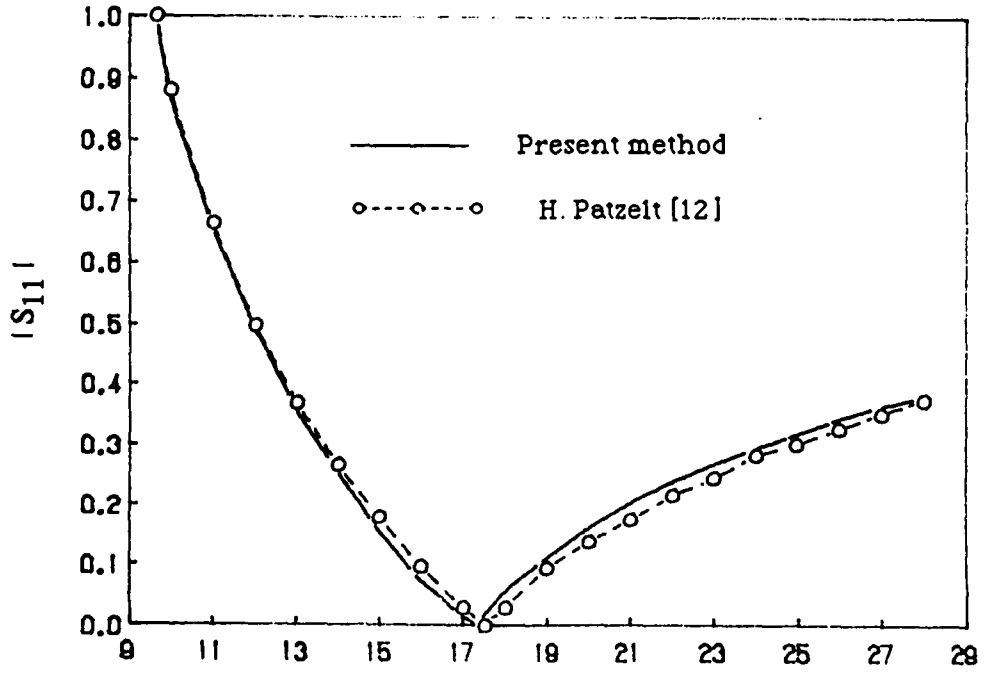

Fig. II-7 Magnitude of reflection coefficient of resonant iris with finite thickness t.
a_1 = 15.8 mm, b_1 = 7.9 mm, a = 11.2 mm, b = 5.6 mm, t = 2 mm

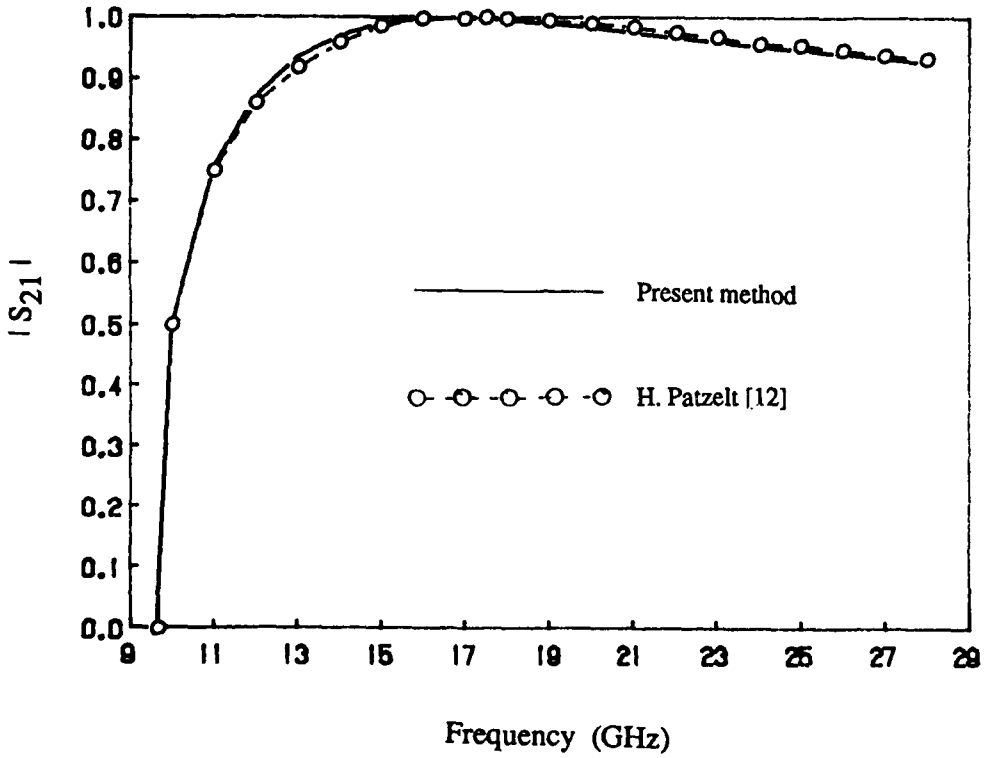

Fig. II-8 Magnitude of transmission coefficient of resonant iris with finite thickness t. a_1 = 15.8 mm, b_1 = 7.9 mm, a = 11.2 mm, b = 5.6 mm, t = 2 mm

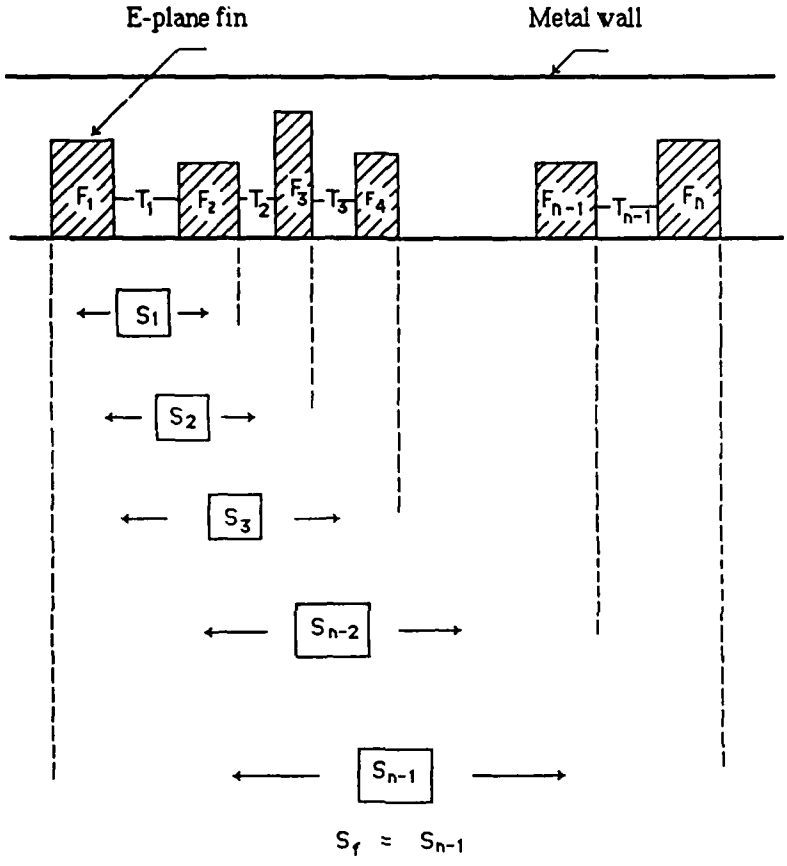

Fig. II-9 A filter contains n non-touching fins.

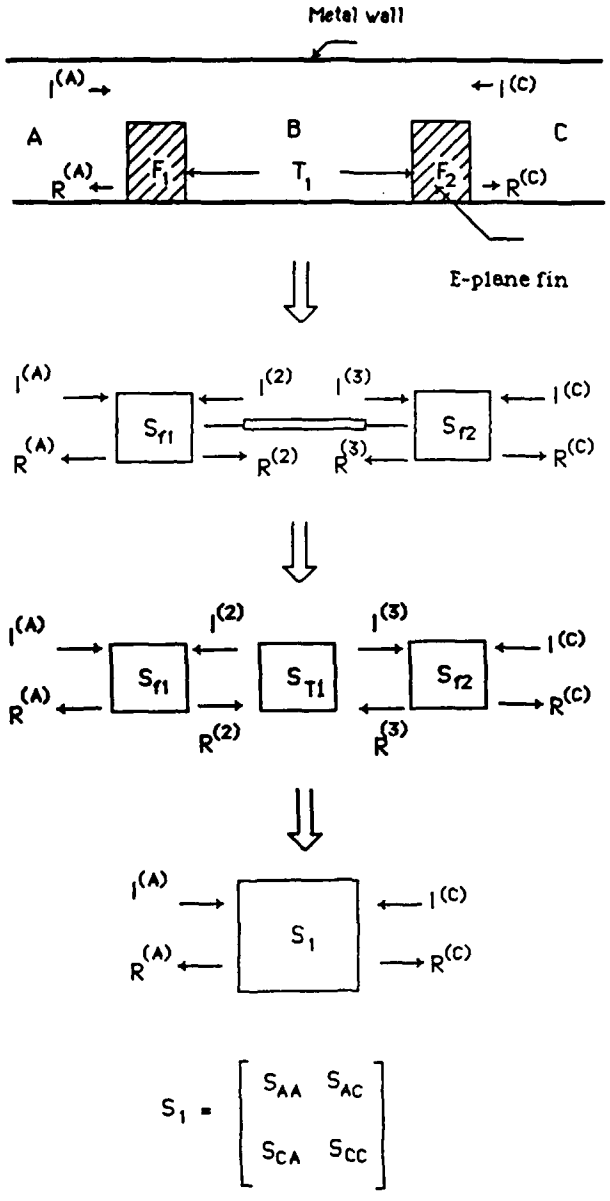

Fig. II-10 Derivation of scattering matrix for the cascaded substructure.

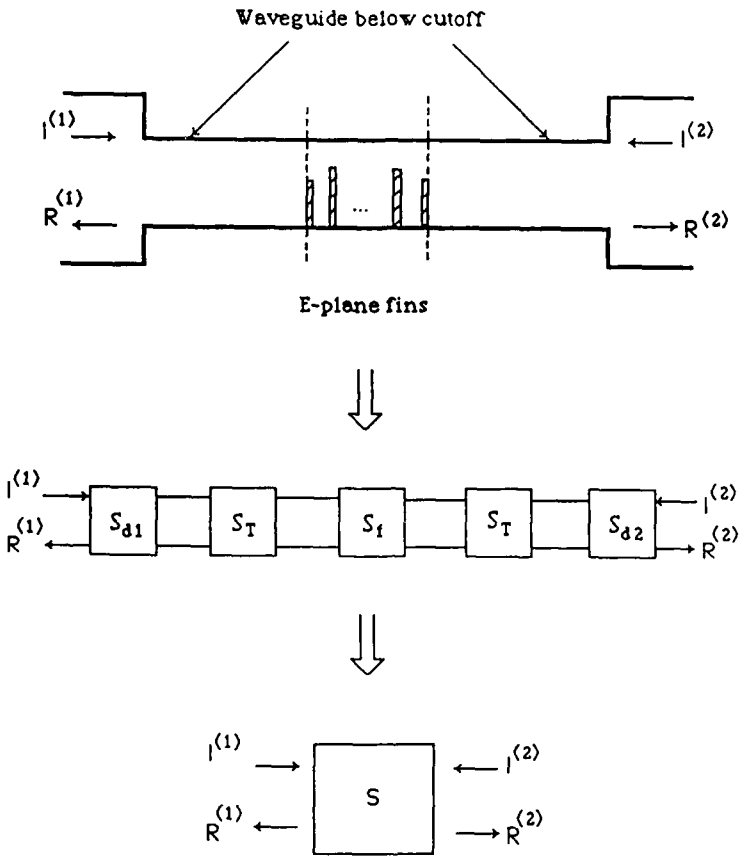

Fig. II-11 Derivation of the final scattering matrix for the filter structure.

fins F_1 and F_2, with spacing T_1. The substructure is shown in Fig. II-10. The scattering matrixes of fins F_1 and F_2, S_{f1} and S_{f2}, are obtained by the method given in Part one. With the scattering matrix notation described above, each of these matrices contains four submatrices and can be written as

$$S_{f1} = \begin{pmatrix} S_{f111} & S_{f112} \\ S_{f121} & S_{f122} \end{pmatrix} \qquad \text{(II-27)}$$

$$S_{f2} = \begin{pmatrix} S_{f211} & S_{f212} \\ S_{f221} & S_{f222} \end{pmatrix} \qquad \text{(II-28)}$$

With the knowledge of the scattering parameters for a single fin, the generalized scattering matrix technique is applied to obtained a scattering matrix of this substructure. The concept is that of multible-reflection phenomenon. If a wave from Region A is incident upon F_1, fields will be partly reflected back into Region A and partly transmitted into Region B. After traveling a distance T_1, a part of the wave transmitted into Region B is reflected back and the remaining part is transmitted into Region C via F_2. This process continues until the reflected wave dies out. This multiple-reflection phenomenon between the F_1 and F_2 implies a matrix combination process that leads to the scattering matrix for the substructure.

In Region B of Fig. II-10, the smaller waveguide section with length T_1, operated below its cutoff frequency, is represented by the matrix S_{T1}. The elements

of those matrices are easily obtained from the transmission line equivalent circuits of the waveguide, in which the characteristic impedances are imaginary. Since no propagation modes exist below cutoff frequency, this waveguide section in the equivalent circuit acts as a lumped reactance. The wave travels a distance T1 in this guide so each mode is multiplied by a exponential decay factor $\exp(-\kappa_{IIzdmn}T_1)$, where d = h or e represent TE or TM waves, respectively. In more detail, S_{T1} can be written as

$$S_{T1} = \begin{bmatrix} \mathbf{0} & \mathbf{S_{t1}} \\ \mathbf{S_{t1}} & \mathbf{0} \end{bmatrix} \qquad \text{(II-29)}$$

where the submatrix S_{t1} is given by

$$S_{t1} = \begin{bmatrix} \exp(-\kappa_{IIzh10}T_1) & 0 & \cdots & 0 \\ 0 & \exp(-\kappa_{IIzh20}T_1) & & \vdots \\ \vdots & & \ddots & \vdots \\ \cdots & & \exp(-\kappa_{IIzePQ}T_1) & 0 \\ 0 & \cdots & 0 & \exp(-\kappa_{IIzePQ}T_1) \end{bmatrix}$$

(II-30)

The combination of S_{t1} with S_{f1} and S_{f2} results in the scattering matrix S_1 in Fig. II-9 that represents the cascaded structure. The algebraic process is shown in Appendix E. The elements of matrix S_1 are given by

$$S_{AA} = S_{f111} + S_{f112}\, S_{t1}\, U_2\, S_{f211}\, S_{t1}\, S_{f121}$$

$$S_{AC} = S_{f112}\, S_{t1}\, U_2\, S_{f212}$$

$$S_{CA} = S_{f221}\, S_{t1}\, U_1\, S_{f121}$$

$$S_{CC} = S_{f222} + S_{f221}\, S_{t1}\, U_1\, S_{f122}\, S_{t1}\, S_{f212}$$

$$U_1 = (\, I - S_{f122}\, S_{t1}\, S_{f211}\, S_{t1})^{-1}$$

$$U_2 = (\, I - S_{f211}\, S_{t1}\, S_{f122}\, S_{t1})^{-1}$$

where **I** is the identity matrix. In the next step, we consider the substructure that consists of fins F_1, F_2, and F_3 with spacing T_1 and T_2. The combination of F_1, F_2, and T_1 is now expressed by matrix S_1. Using S_{T2} and S_{f3} to represent scattering matrices of T_2 and F_3 respectively, we obtain the matrix S_2 of this substructure in the same way as that of deriving matrix S_1. The same procedure is repeated until the matrix S_f is obtained (Fig. II-9).

D. SCATTERING MATRIX REPRESENTATION OF CASCADED SECTIONS

The side view of the filter can be now represented by Fig.II-11. The double-step junctions are described by scattering matrices S_{d1} and S_{d2}. The capacitive element of the filter is the portion of the non-touching E-plane fins, which is represented by scattering matrices S_f. The matrix S_T represents the evanescent mode guide section, and it can be found in the same way as S_{T1}. Since S_{d1}, S_{d2},

S_f, and S_T are all known, the overall matrix S, which characterizes the filter structure, can be determined from these scattering matrices by the generalized scattering matrix technique. The elements of the matrix S are given by :

$$\begin{bmatrix} R^{(1)} \\ R^{(2)} \end{bmatrix} = \begin{bmatrix} S_{11} & S_{12} \\ S_{21} & S_{22} \end{bmatrix} \begin{bmatrix} I^{(1)} \\ I^{(2)} \end{bmatrix} \qquad \text{(II-31)}$$

where the submatrices S_{11}, S_{12}, S_{21}, and S_{22} are repraesented by:

$$S_{11} = S_{d111} + S_{d112}\, SD^{-1} SU$$

$$S_{12} = S_{d112} + SD^{-1} SV$$

$$S_{21} = S_{d112} + SD^{-1} SP$$

$$S_{22} = S_{d111} + S_{d112}\, SD^{-1} SQ$$

$$SD = (I - S_t S_{f11} S_t S_{d122}) (I - S_t S_{f22} S_t S_{d211}) - S_t S_{f12} S_t S_{d211}\ S_t S_{f21} S_t S_{d122}$$

$$SU = S_t S_{f11} S_t S_{d121} (I - S_t S_{f22} S_t S_{d211}) + S_t S_{f12} S_t S_{d211}\ S_t S_{f21} S_t S_{d121}$$

$$SV = S_t S_{f12} S_t S_{d212} (I - S_t S_{f22} S_t S_{d211}) + S_t S_{f12} S_t S_{d211}\ S_t S_{f22} S_t S_{d212}$$

$$SP = (I - S_t S_{f11} S_t S_{d122}) S_t S_{f21} S_t S_{d121} + S_t S_{f11} S_t S_{d121}\ S_t S_{f21} S_t S_{d122}$$

$$SQ = (I - S_t S_{f11} S_t S_{d122}) S_t S_{f22} S_t S_{d212} + S_t S_{f12} S_t S_{d212}\ S_t S_{f21} S_t S_{d122}$$

III DESIGN EXAMPLES AND DISCUSSIONS

The behavior of a waveguide below cutoff is basically that of an inductive element. Capacitive elements are needed for a bandpass filter. The non-touching E-plane fin may be represented by its equivalent Γ-network (Fig. I-2 (d)). The element values in the equivalent network can be found from S_f. In principle, the width and height of the fin have to be chosen such that X_2 (in Fig. I-2 (d)) is negative, equivalent to a shunt capacitor.

Several filters have been designed by the procedure described above. The design procedure can be used in a wide frequency range. Howevre in this study, only bandpass filters operating in Ka band have been considered. In the following discussion, the larger waveguide is WR-28 (7.11 mm × 3.56 mm) while the smaller waveguide is WR-15 (3.76 mm × 1.88 mm). The center frequency is the most important quantity for design of a bandpass filter. Attention is first directed to how the height and width of the single fin, and the distance between the edge of the fin and the step junction affect the center frequency of the evanescent filter.

Figure. II-12 shows the relationship between the height of the fin and the center frequency for a filter with the E-plane fin supported by a Duroid substrate (dielectric constant $\varepsilon = 2.2$, thickness $h_2 = 0.127$ mm). The center frequency decreases as the height d of the fin increases, because as d increases there is more electric energy stored in the gap between the fin and the wall of the guide. This corresponds to a larger shunt capacitor in its equivalent network while the series

inductance X_1 exhibits little change.

Figures II-13 (a) and (b) show the relationship between the width of the fin and the center frequency for a fin with a fixed height. The wider the fin, the lower the center frequency is. The wider fin leads to a larger capacitance and inductance in its equivalent circuit and hence a lower resonant frequency. (See Fig. I-12)

The insertion loss versus the frequency for different distance T of the filter with fixed width and height of the fin is shown in Figs. II-14 and II-15. In Fig. II-14 the fin is supported by a Duroid substrate while in Fig. II-15 there is no dielectric substrate. When the fin is separated away from the step junction, the center frequency becomes higher and the curve becomes steeper. This phenomenon can be explained as following. To simplify our discussing, we assume that only the TE_{10} evanescent mode exists in the smaller guide containing a narrow fin without substrate. The waveguide can be described by a simple transmission line equivalent circuit with imaginary characteristic impedance $Z_o = jX_o$ (Fig. II-16 (a)), or in terms of its π–equivalent network as shown in Fig. II-16 (b). The fin is represented by the equivalent T-network (Fig. II-16 (c)). If the value of X_1 is small compared to X_o, then the equivalent circuit of the filter may be expressed by Fig. II-16 (d), where X_o is given by

$$X_o = 120b\pi / (a\sqrt{(\lambda/\lambda_c)^2 - 1}) \qquad (II\text{-}32)$$

The propagation canstant of the TE_{10} mode, γ, is given by

$$\gamma = 2\pi\sqrt{(\lambda/\lambda_c)^2 - 1} / \lambda \qquad (II\text{-}33)$$

in which λ is the free-space wavelength and λ_c is the cutoff wavelength.

The resonant frequency of the filter in Fig. II-16 (d) is mainly determined by X_2 and the parallel inductance $L_p = jX_o \coth(0.5\gamma T)$. When T becomes larger, L_p becomes smaller while X_2 is unchanged. Hence the resonant frequency becomes higher. If T is large enough, L_p approaches to jX_o since the term of $\coth(0.5\gamma T)$ tends to 1. Hence for large T, the center frequency of the filter approaches to a certain value. Also the curve becomes sharper when T increases, since the coupling between the fin and the step is weaker.

With the data presented above, it is now possiple to design a filter with one fin element. Fig. II-17 shows the results for a filter designed in Ka band using one fin element without a dielectric layer. The solid curve represents the results obtained by this analysis and the dashed line indicates the measured data. They are in good agreement. Figure II-18 shows the results of the filter with the E-plane fin supported by a Duroid layer. Once again agreement between theoretical prediction and experimental data is quite good. The small deviation of the insertion loss between theory and experiment at the center frequency comes from the metal and dielectric loss.

Figure II-19 shows the calculated response of a filter that consists of two equal E-plane fin elements on a Duriod substrate. The height of the fin, the distance from the edge of the fin to the double-step junction, and the spacing of the two fins are the design parameters. The 3 dB bandwidth is about 1.6 GHz. It is noted that the steepness of the out-of-band insertion loss curve on the higher frequency side in

Fig. II-19 is almost equal to the one on the lower frequency side. This happens because the waveguide below its cutoff frequency acts like a lumped reactance.

In general, wider bandwidth and better transmission performance can be achieved by increasing the number of fins. For a multi-fin structure an optimization procedure similar to [16] may be used to optimize the performance of the filter. Alternatively, a filter synthesis can be used to find the required equivalent circuit parameters in the filter. The necessery fin dimensions and fin spacing can be found from a look-up table. The center frequency can be controlled by the dimensions of the fins and the distance between edge of the fin and the double-step junction. The shorter the height and the narrower the width, the higher the center frequency. Also a longer distance from the edge of the fin to the double-step junction leads to a higher central frequency. The height of the fin is the most sensitive parameter to the center frequency. For instance, in Figs. II-13 (a) and (b), if the width of the fin chages by 0.1 mm, the certer frequency shifts about 0.5 GHz, while the variation of 0.05 mm on the height corresponts to about 1 GHz frequency changing (See Figs. II-12 (a) and (b)).

Since the non-touching fins can be produced by photolithographic techniques, fine tuning is normally not required.

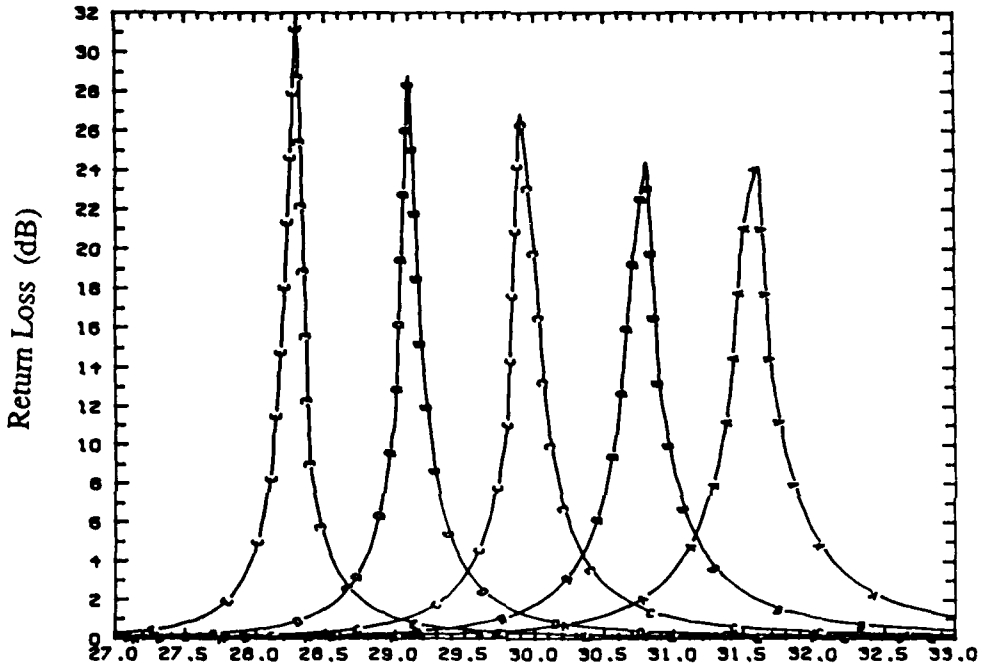

Fig. II-12 (a) Return loss of the filter versus frequency for different height d of the E-plane fin. h1 = 1.753 mm, h2 =0.127 mm, ε_2 = 2.2 w = 0.3 mm, T = 2.0 mm, A : d = 1.4 mm, B: d =1.45 mm, C : d = 1.50 mm, D : d = 1.55 mm, E : d = 1.60 mm

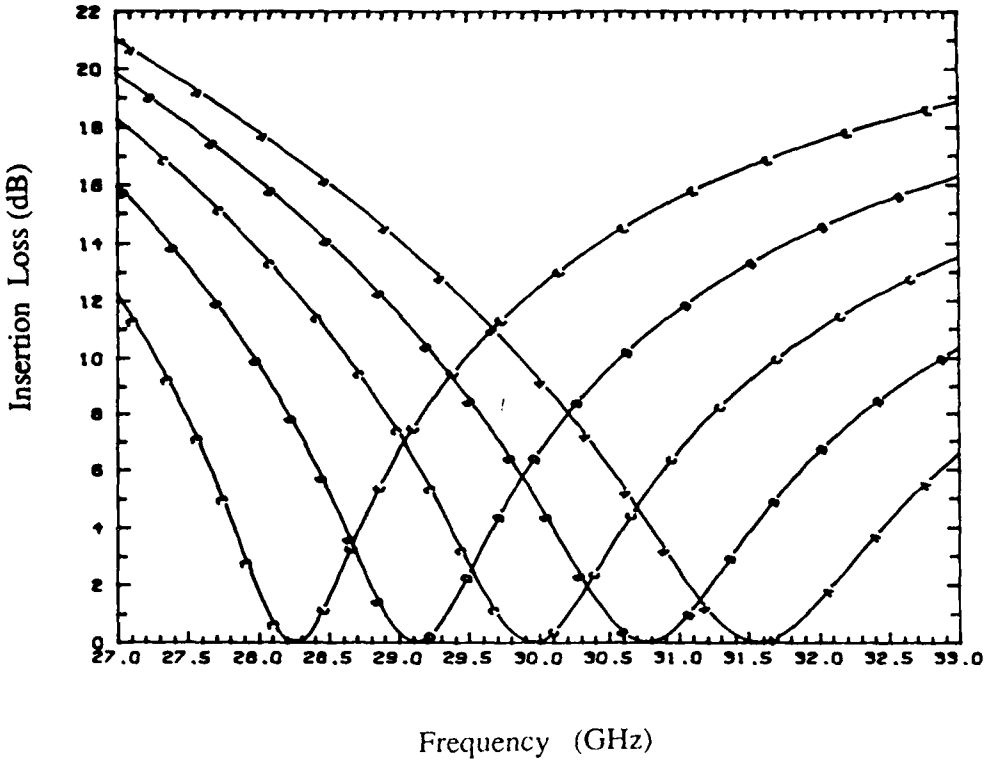

Fig. II-12 (b) Insertion loss of the filter versus frequency for different height d of the E-plane fin. h1 = 1.753 mm, h2 =0.127 mm, ε_2 = 2.2 w = 0.3 mm, T = 2.0 mm, A : d = 1.4 mm, B: d =1.45 mm
C : d = 1.50 mm, D : d = 1.55 mm, E : d = 1.60 mm

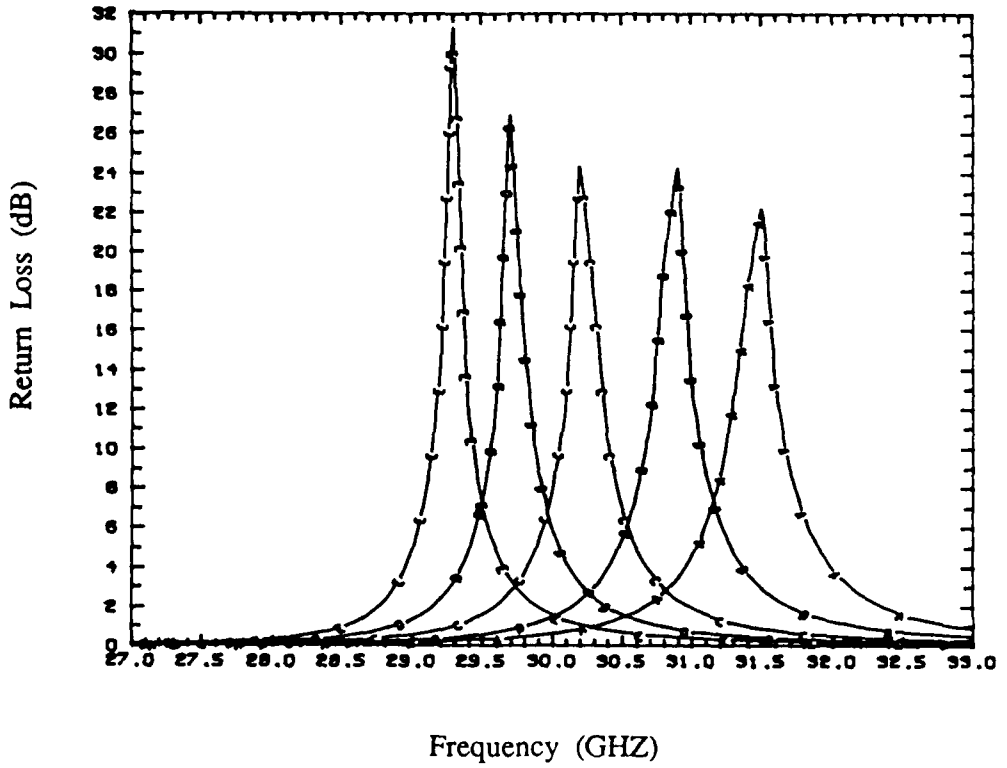

Fig. II-13 (a) Return loss versus frequency for different width of E-plane fin

d = 1.483mm, T = 2.0mm, A : w = 0.1mm, B: w =0.2mm

C : w = 0.3mm, D : w = 0.4mm, E : w = 0.5mm

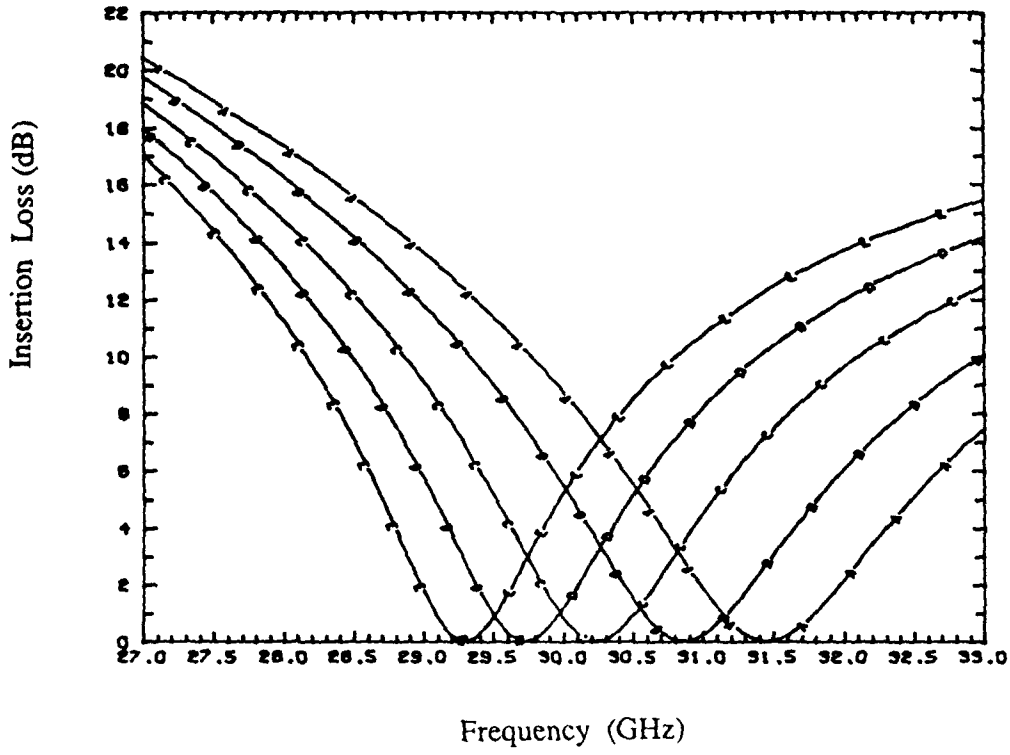

Fig. II-13 (b) Insertion loss of the filter versus frequency for different width w of E-plane fin. h1 = 1.753 mm, h2 =0.127 mm, ε_2 = 2.2, d = 1.483 mm, T = 2.0 mm, A : w = 0.1mm, B: w =0.2 mm C : w = 0.3 mm, D : w = 0.4 mm, E : w = 0.5 mm

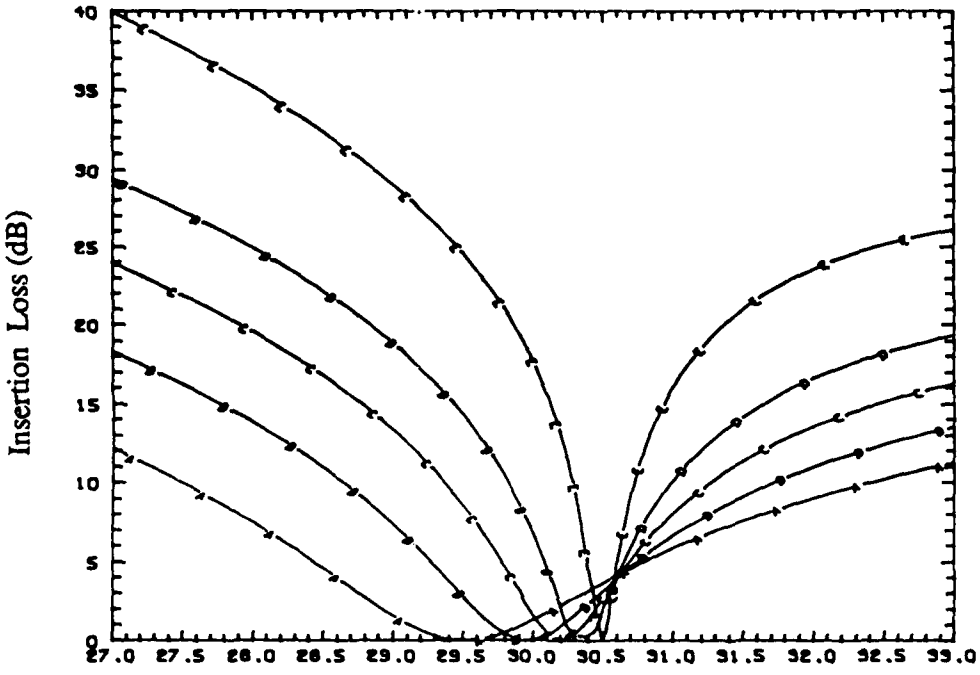

Fig. II-14 Return loss versus frequency for different T, the distance between step junction and E-plane fin with Duriod substrate.

d = 1.50mm, w = 0.3mm, A : T = 1.5mm, B: T = 2.0mm

C : T = 2.5mm, D : T = 3.0mm, E : T = 4.0mm

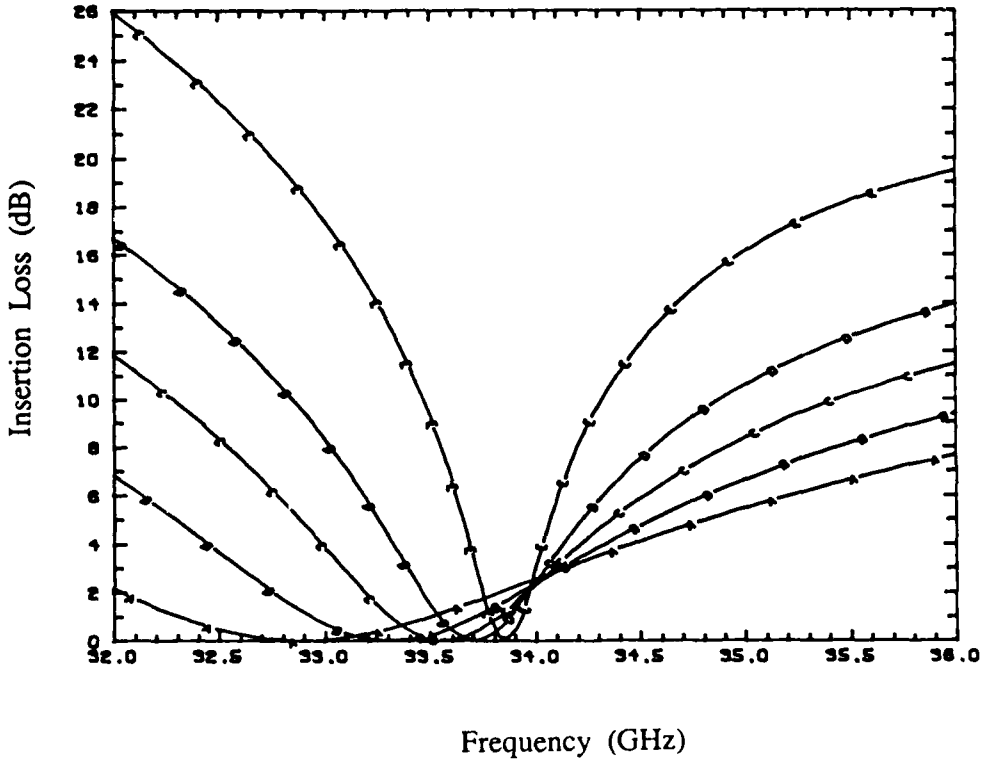

Fig. II-15 Insertion loss of the filter versus frequency for different distance T between the step junction and the E-plane fin (metal only).
d = 1.50 mm, w = 0.28 mm, A : T = 1.5 mm, B: T = 2.0 mm
C : T = 2.5 mm, D : T = 3.0 mm, E : T = 4.0 mm

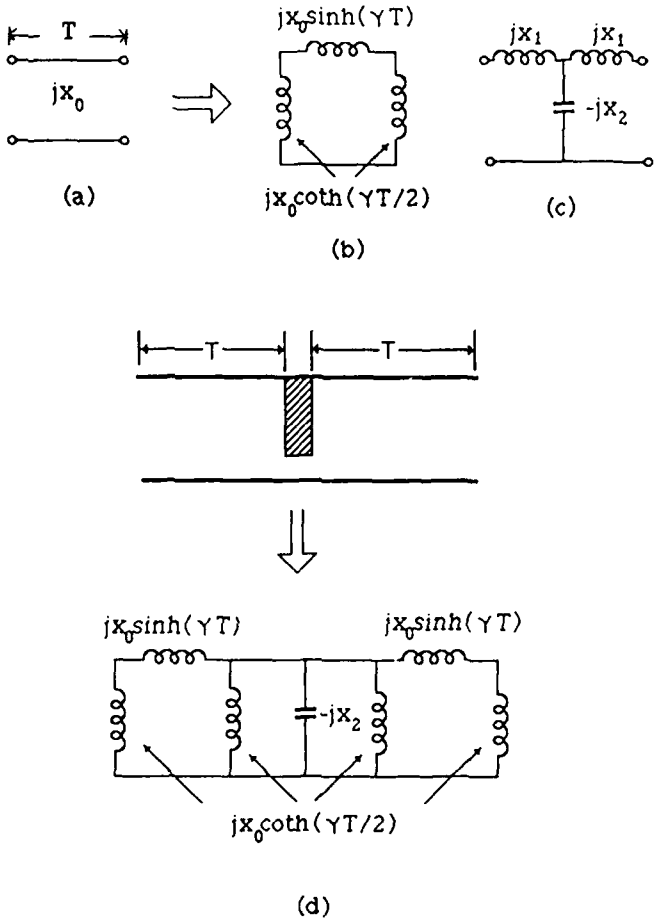

Fig. II-16

(a) Transmission line equivalent circiut for evanescent mode waveguide

(b) π–network equivalent circiut for evanescent mode waveguide

(c) T–network equivalent circiut for metal fin

(d)A simplified euqivalent circuit of the evanescent mode waveguide filter

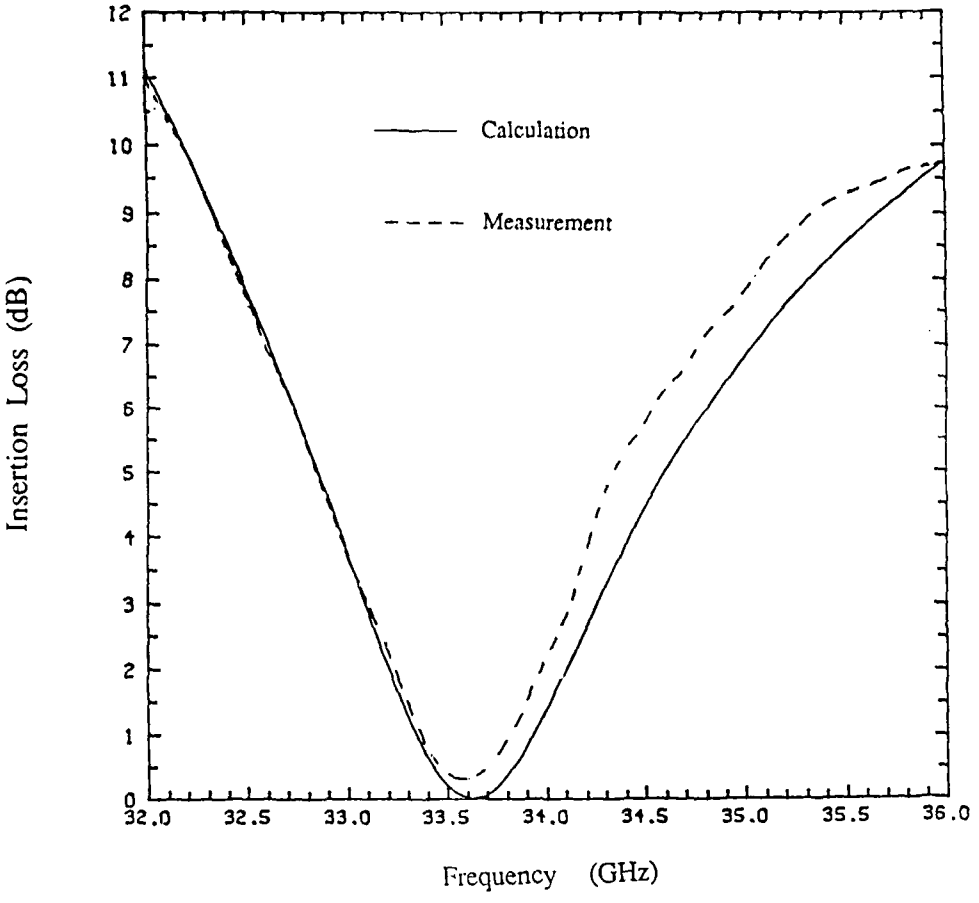

Fig. II-17 Computed and measured insertion loss for an evanescent mode waveguide filter with an E-plane fin. (metal only, h_1 = 1.753 mm, h_2 = 0.157 mm, d = 1.511 mm, w = 0.287 mm, T = 2.506 mm)

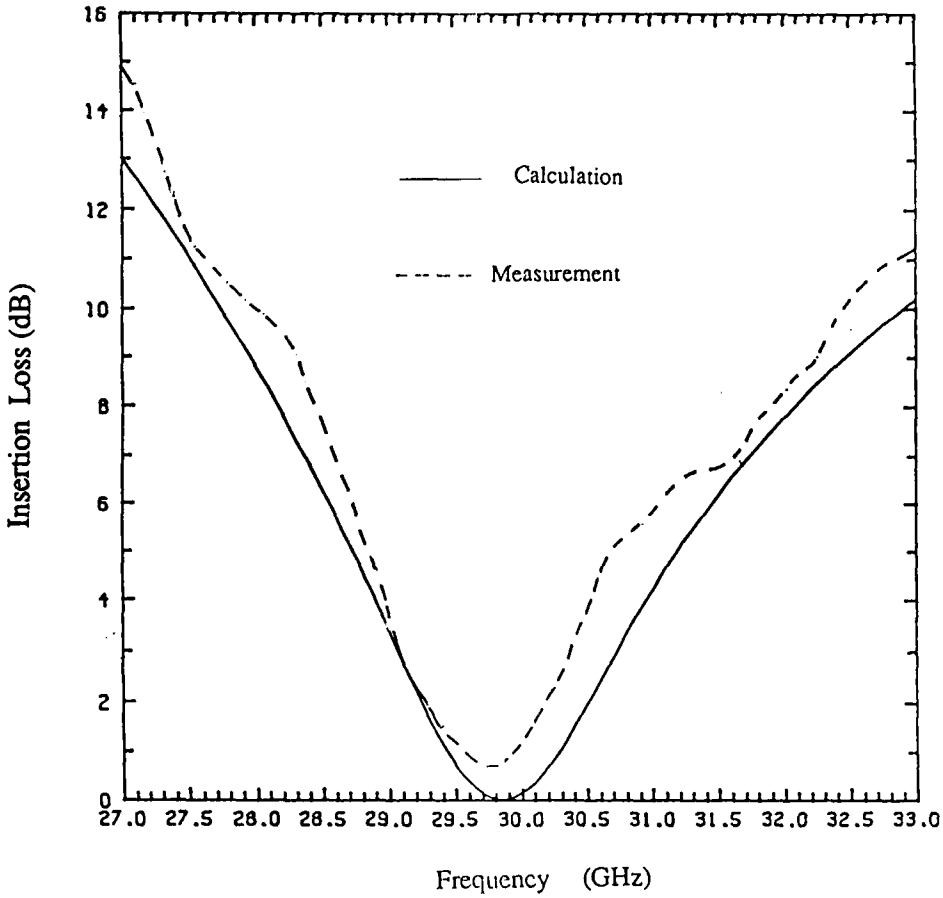

Fig. II-18 Computed and measured insertion loss for an evanescent mode waveguide filter with an E-plane fin on a Duriod substrate. (h_1= 1.753 mm, ε_2 =2.2, h_2 = 0.157 mm, d = 1.483 mm, w = 0.292 mm, T = 1.502 mm)

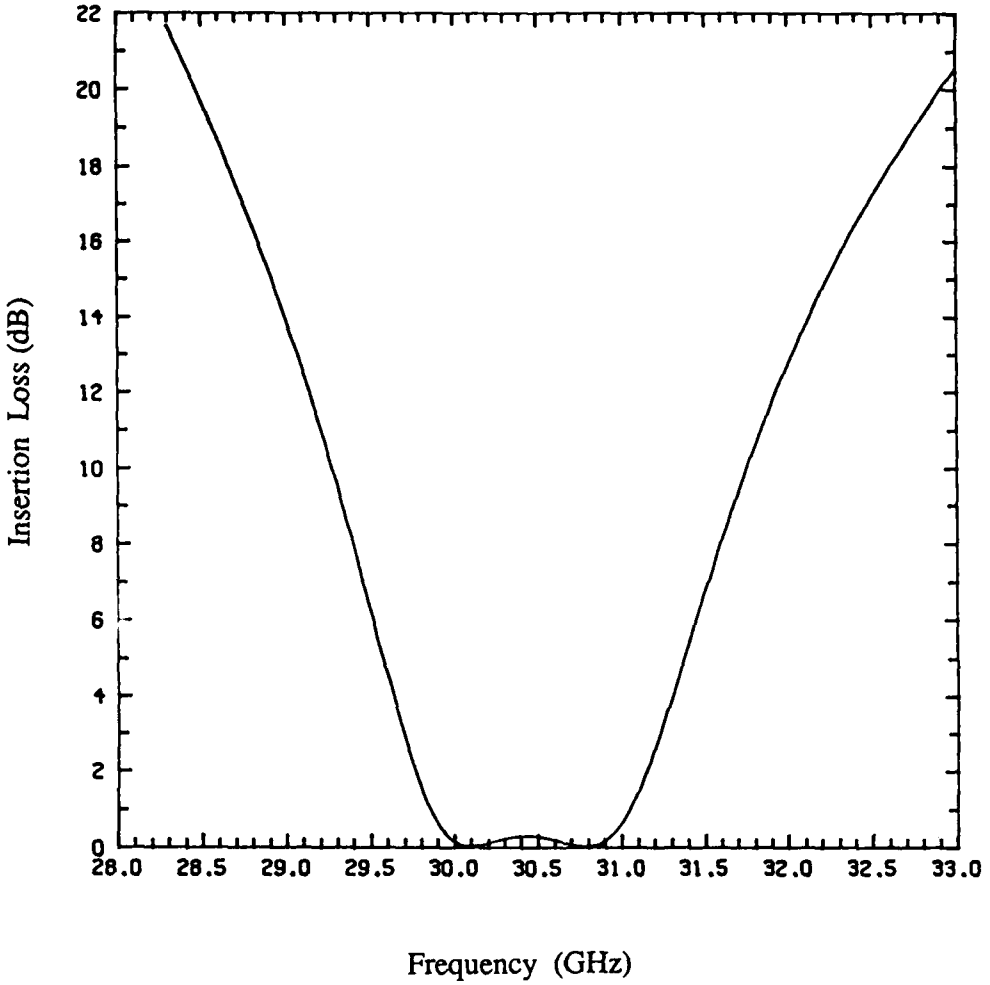

Fig. II-19 (a) Insertion loss for an evanescent mode waveguide filter with two E-plane fins on a Duriod substrate. (h_1= 1.753 mm, h_2 = 0.127 mm, d = 1.50 mm, w = 0.292 mm, T = 2.0 mm, T1= 4.6248 mm, ε_2 = 2.2)

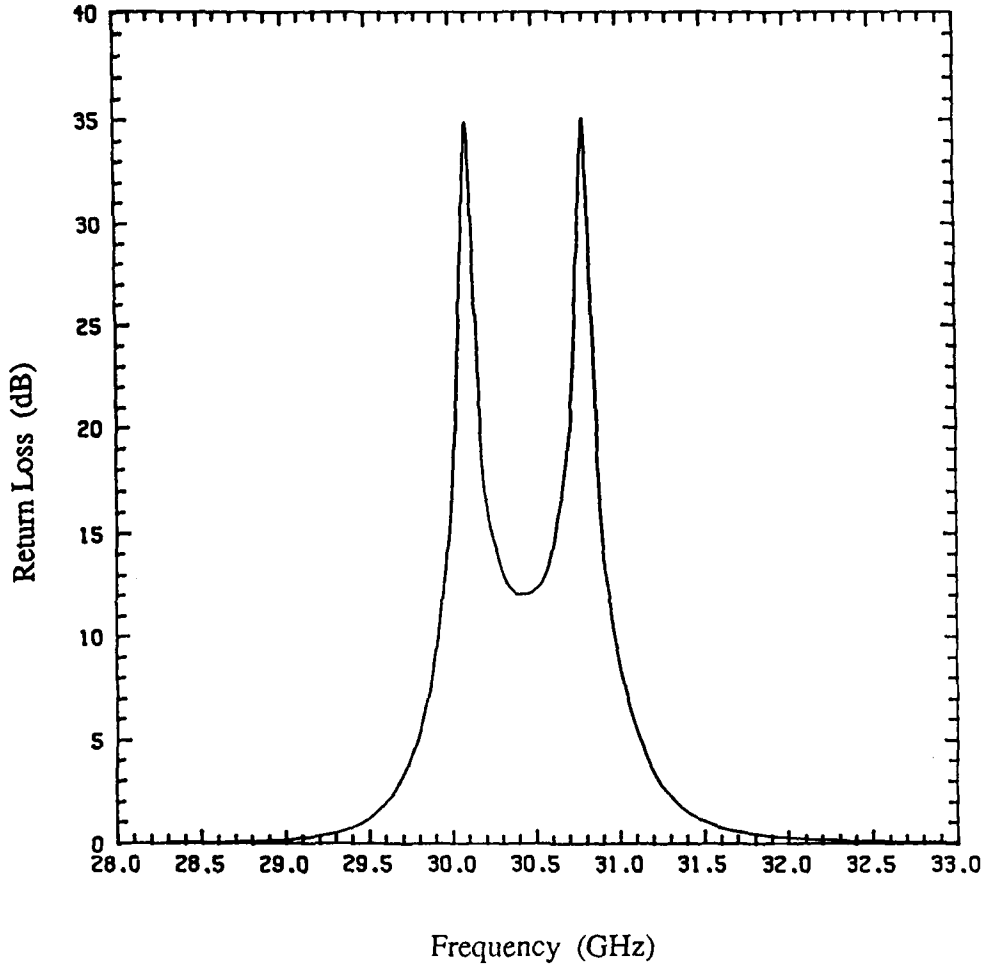

Fig. II-19 (b) Return loss for an evanescent mode waveguide filter with two E-plane fins on a Duriod substrate. (h_1= 1.753 mm, h_2 = 0.127 mm, d = 1.50 mm, w = 0.292 mm, T = 2.0 mm, T1= 4.6248 mm, ε_2 = 2.2)

IV CONCLUSIONS

The analysis and design of evanescent mode waveguide filters with non-touching E-plane fins are presented. In the analysis, the fundamental mode as well as the higher order modes effects have been taken into account. This is important in an accurate filter design. The filter designed in Ka band has been tested and good agreement between the measurement and the theory is observed. It is believed that this kind of filter will be useful in the millimeter-wave frequency region.

APPENDIX A. CLOSED FORM EXPRESSION OF GREEN'S FUNCTION IN THE SPECTRAL DOMAIN

According to [9], the TM-to-x (LSM) and TE-to-x (LSE) equivalent transmission lines for the E-plane strip described in Fig. 2 can be drawn in Fig. A-1. Here,

$$\gamma_i = \sqrt{\alpha_n^2 + \beta^2 - \epsilon_i k^2} \qquad (A-1)$$

$$Z_{TMi} = \frac{\gamma_i}{j\omega\epsilon_0\epsilon_i} \qquad (A-2)$$

$$Z_{TEi} = -\frac{j\omega\mu}{\gamma_i} \qquad i=1,2,3, \quad n=0,1,2,3\cdots. \qquad (A-3)$$

The driving point input impedance Z^e for the TM equivalent circuit is given by

$$Z^e = \frac{1}{y_2^e + y_{2\gamma}^e} \qquad (A-4)$$

where

$$y_{2\gamma}^e = y_{TM3}\cdot\coth\gamma_3 h_3 \qquad (A-5)$$

$$y_2^e = y_{TM2}\frac{y_{TM2} + y_1^e\coth\gamma_2 h_2}{y_1^e + y_{TM2}\coth\gamma_2 h_2} \qquad (A-6)$$

$$y_1^e = y_{TM1}\coth\gamma_1 h_1. \qquad (A-7)$$

Notice that y^e and y^e are input admittances looking left at $x = h_1$ and $x = h_1 + h_2$, respectively, while y^e_{2r} is the admittance looking right at $x = h_1 + h_2$. Similar equations can be written for the TE equivalent circuit:

$$Z^h = \frac{1}{y_2^h + y_{2Y}^h} \qquad (A-8)$$

$$y_{2Y}^h = y_{TE3}\coth\gamma_3 h_3 \qquad (A-9)$$

$$y_1^h = y_{TE1}\coth\gamma_1 h_1 \qquad (A-10)$$

$$y_2^h = y_{TE2}\frac{y_{TE2} + y_1^h \coth\gamma_2 h_2}{y_1^h + y_{TE2}\coth\gamma_2 h_2}. \qquad (A-11)$$

Finally, the Green,s functions in the spectral domain can be represented by Z^h and Z^e as follows [8]:

$$\tilde{G}_{yy} = Z^e N_z^2 + Z^h N_y^2 \qquad (A-12)$$

$$\tilde{G}_{yz} = \tilde{G}_{zy} = (Z^e - Z^h) N_z N_y \qquad (A-13)$$

$$\tilde{G}_{zz} = Z^h N_z^2 + Z^e N_y^2 \qquad (A-14)$$

where

$$N_y = \frac{\alpha_n}{\sqrt{\alpha_n^2 + \beta^2}}, \qquad N_z = \frac{\beta}{\sqrt{\alpha_n^2 + \beta^2}} \qquad (A-15)$$

Note that the denominators of Z^h and Z^e are the eigenvalue equationn of LSE and LSM modes.

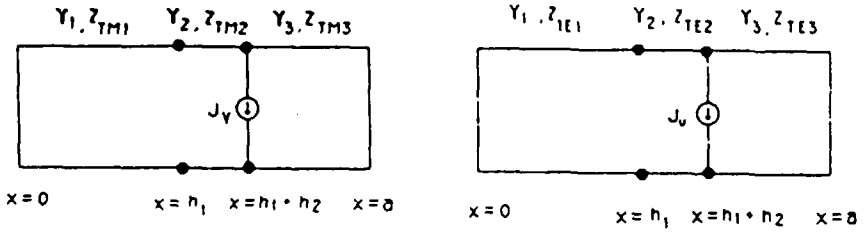

Fig. A-1 The TM and TE equivalent transmission lines for the E-plane strip

APPENDIX B. EXPRESSION OF NORMALIZED REACTANCE X_1 AND X_2

The equivalent circuit element values of the non-touching E-plane fin are derived as follows. In Fig. B-1, the normalized input inpedance Z_{in} can be expressed as

$$\begin{aligned} Z_{in} &= j X_1 + Z'' \\ &= j X_1 + \frac{j X_2 (1 + j X_1)}{1 + j (X_1 + X_2)} \\ &= \frac{j X_1 - X_1 (X_1 - X_2) + j X_2 (1 + j X_1)}{1 + j (X_1 + X_2)} \\ &= \frac{1}{G_{in} + j B_{in}} \end{aligned} \qquad (B-1)$$

where

$$G_{in} + j B_{in} = \frac{1 + j (X_1 + X_2)}{j (X_1 + X_2) - X_1 (X_1 + 2X_2)} \qquad (B-2)$$

Equation (B-2) can be repressed as

$$\begin{aligned} 1 + j (X_1 + X_2) = {} & j G_{in} (X_1 + X_2) - B_{in} (X_1 + X_2) \\ & - G_{in} X_1 (X_1 + 2X_2) - j B_{in} X_1 (X_1 + X_2) \end{aligned} \qquad (B-3)$$

The real part and imaginary part of the left hand side of the Eq. (B-3) should be equal to those of the right hand side, a set of coupled equations is obtaind:

$$G_{in}(X_1 + X_2) - B_{in}X_1(X_1 + X_2) = (X_1 + X_2) \qquad (B\text{-}4)$$

$$B_{in}(X_1 + X_2) + G_{in}X_1(X_1 + 2X_2) = -1 \qquad (B\text{-}5)$$

X_1 and X_2 are found by solving the Eqs. (B-4) and (B-5). The result is given by:

$$X_2 = \pm\left[\left(\frac{B_{in}}{B_{in}^2 + G_{in}^2 - G_{in}}\right)^2 + \frac{G_{in} - 1}{B_{in}^2 + G_{in}^2 - G_{in}}\right]^{1/2} \qquad (B\text{-}6)$$

$$X_1 = \frac{B_{in}}{G_{in} - (B_{in}^2 + G_{in}^2)} \mp X_2. \qquad (B\text{-}7)$$

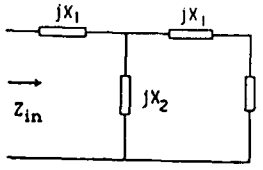

$Z_1 = 1$

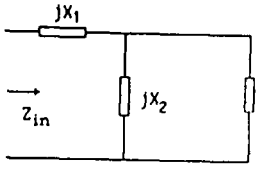

$Z_1' = 1 + j X_1$

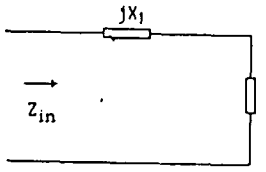

$$Z_1'' = \frac{j X_2 (1 + j X_1)}{1 + j (X_1 + X_2)}$$

Fig. B-1 Equivalent circuit to find the normalized input impedance.

APPENDIX C. NORMALIZED COEFFICIENTS OF THE EIGENFUNCTIONS IN REGION II

In reference to Fig. II-4 and Eqs. II-3 and II-4, the tangential fields in Region II are given by

$$E_{IIy} = -\partial\phi_2 / \partial z + (1 / j\omega\varepsilon_o\varepsilon_j)\,\partial^2\psi_2 / \partial x\partial y$$

$$= -\sum_{m=1}^{\infty}\sum_{n=0}^{\infty} k_{IIzhmn}(-A_{IImn} + B_{IImn})\,P_{IImn} -$$

$$(1/j\omega\,\varepsilon_j\,\varepsilon_o)\sum_{m=0}^{\infty}\sum_{n=1}^{\infty}(n\pi/b)\cos[n\pi/b(y-y_1)]\,(-C_{IImn} + D_{IImn})\,\partial T_m/\partial x \qquad (C\text{-}1)$$

$$E_{IIz} = \partial\phi_{II} / \partial y + (1 / j\omega\varepsilon_o\varepsilon_j)\,\partial^2\psi_{II} / \partial x\partial z$$

$$= -\sum_{m=1}^{\infty}\sum_{n=0}^{\infty}(n\pi/b)\sin[n\pi/b(y-y_1)]\,(-A_{IImn} + B_{IImn})\,R_{IImn} +$$

$$(1/j\omega\varepsilon_o)\sum_{m=0}^{\infty}\sum_{n=1}^{\infty} k_{IIzemn}\,(-C_{IImn} + D_{IImn})\,n\sin[n\pi/b(y-y_1)]\,\partial T_m/\partial x / \varepsilon_j \qquad (C\text{-}2)$$

$$H_{IIy} = \partial\psi_{II} / \partial z + (1 / j\omega\mu_o)\,\partial^2\phi_{II} / \partial x\partial y$$

$$= \sum_{m=0}^{\infty}\sum_{n=1}^{\infty} k_{IIzemn}(-C_{IImn} + D_{IImn})\,Q_{IImn} -$$

$$(1 / j\omega\mu_o)\sum_{m=1}^{\infty}\sum_{n=0}^{\infty}(n\pi/b)\sin[n\pi/b(y-y_1)]\,(A_{IImn} + B_{IImn})\,\partial R_m/\partial x \qquad (C\text{-}3)$$

$$H_{IIz} = -\partial\psi_{II} / \partial y + (1 / j\omega\mu_o)\, \partial^2\phi_{II} / \partial x\partial z$$

$$= -\sum_{m=0}^{\infty}\sum_{n=1}^{\infty} (n\pi/b)\cos[n\pi/b(y-y_1)]\,(C_{IImn} + D_{IImn})\, T_{IImn} +$$

$$(1 / j\omega\mu_o)\sum_{m=1}^{\infty}\sum_{n=0}^{\infty} k_{IIzhmn}\,(-A_{IImn} + B_{IImn})\sin[n\pi/b(y-y_1)]\,\partial R_m / \partial x \qquad (C\text{-}4)$$

where

$$A_{IImn} = a_{IImn}\exp(-k_{IIzhmn}z)\,, \qquad B_{IImn} = b_{IImn}\exp(k_{IIzhmn}z)$$

$$C_{IImn} = c_{IImn}\exp(-k_{IIzemn}z)\,, \qquad D_{IImn} = d_{IImn}\exp(k_{IIzemn}z) \qquad (C\text{-}5)$$

The following equations are obtained by matching the tangential fields at the interface $x = x_1 + h_1$ and $x = x_1 + h_1 + h_2$.

$$\bar{N}_{rII2m} = N_{rII1m}\sin(k_{IIx1hm}\, h_1) \qquad (C\text{-}6)$$

$$k_{IIx2em}\,\bar{N}_{tII2m} = -k_{IIx1em}\, N_{tII1m}\sin(k_{IIx1em}\, h_1) \qquad (C\text{-}7)$$

$$\varepsilon_2\, N_{tII2m} = \varepsilon_1 N_{tII1m}\cos(k_{IIx1em}\, h_1) \qquad (C\text{-}8)$$

$$k_{IIx2hm}\, N_{rII2m} = k_{IIx1hm}\, N_{rII1m}\cos(k_{IIx1hm}\, h_1) \qquad (C\text{-}9)$$

$$-N_{rII3m}\sin(k_{IIx3hm}\, h_3)$$

$$= N_{rII2m}\sin(k_{IIx2hm}\, h_2) + N_{rII2m}\cos(k_{IIx2hm}\, h_2) \qquad (C\text{-}10)$$

$$k_{IIx3em}\, N_{tII3m}\sin(k_{IIx3em}\, h_3$$

$$= -k_{IIx2em}\,[N_{tII2m}\sin(k_{IIx2em}\, h_2) - \bar{N}_{tII2m}\cos(k_{IIx2em}\, h_2)] \qquad (C\text{-}11)$$

$$-\varepsilon_3 N_{tII3m}\cos(k_{IIx3em}\, h_3)$$

$$= \varepsilon_2[\, N_{tII2m}\cos(k_{IIx2em}\, h_2) + \bar{N}_{tII2m}\sin(k_{IIx2em}\, h_2)] \qquad (C\text{-}12)$$

$$k_{IIx3hm}\, N_{rII3m}\cos(k_{IIx3hm}\, h_3)$$

$$= k_{IIx2hm}\,[N_{rII2m}\cos(k_{IIx2hm}\, h_2) - \bar{N}_{rII2m}\sin(k_{IIx2em}\, h_2)] \qquad (C\text{-}13)$$

The coefficients N_{rIIj} and N_{tIIj} are normalized such that

$$\int_{x_1}^{x_1+a} R_{IIm}(x)\, dx = 1 \quad \text{and} \quad \int_{x_1}^{x_1+a} T_{IIm}(x)\, dx = 1 \qquad (C\text{-}14)$$

Normalization leads to the results

$$N_{rII1m} = 0.5\,(1+\delta_{mo})\,\{\,[\,0.5h_1 - 0.25\sin(2\,k_{IIx1hm}\, h_1)/\,k_{IIx1hm}\,] +$$
$$[\,k_{IIx3hm}\cos(\,k_{IIx3hm}\, h_3)]^2$$
$$[\,k_{IIx1hm}\cos(\,k_{IIx1hm}\, h_1)\cos(\,k_{IIx2hm}\, h_2) -$$
$$k_{IIx2hm}\sin(\,k_{IIx1hm}\, h_1)\sin(\,k_{IIx2hm}\, h_2)\,]^2[0.5h_3 -$$
$$0.25\sin(2\,k_{IIx3hm}\, h_3)/\,k_{IIx3hm}\,] + [\sin(\,k_{IIx1hm}\, h_1)]^2$$
$$[\,0.5h_2 + 0.25\sin(2\,k_{IIx2hm}\, h_2)/\,k_{IIx2hm}\,] +$$
$$[\,k_{IIx1hm}\cos(\,k_{IIx1hm}\, h_1)/\,k_{IIx2hm}\,]^2$$
$$[\,0.5h_2 - 0.25\sin(2\,k_{IIx2hm}\, h_2)/\,k_{IIx2hm}\,] +$$
$$\sin(\,k_{IIx1hm}\, h_1)\,k_{IIx1hm}\cos(\,k_{IIx1hm}\, h_1)/\,k_{IIx2hm}$$
$$[\,\sin(\,k_{IIx2hm}\, h_2)]^2\,\}^{-1/2} \qquad (C\text{-}15)$$

$$N_{tII1m} = 0.5\,(1+\delta_{mo})\,\{\,[\,0.5h_1 + 0.25\sin(2\,k_{IIx1em}\,h_1)/\,k_{IIx1em}\,]\,/\,\varepsilon_1 +$$

$$[\varepsilon_3\cos(k_{IIx3em}\,h_3)]^{-2}\,[\,\varepsilon_1\cos(k_{IIx1em}\,h_1)\cos(k_{IIx2em}\,h_2) -$$

$$\varepsilon_2\,k_{IIx1em}\sin(k_{IIx1em}\,h_1)\sin(k_{IIx2em}\,h_2)\,/\,\varepsilon_1\,k_{IIx2em}\,]^{\,2}/\,\varepsilon_3$$

$$[0.5h_3 + 0.25\sin(2\,k_{IIx3em}\,h_3)/\,k_{IIx3em}\,] +$$

$$[\,-k_{IIx1em}\,h\sin(k_{IIx1em}\,h_1)\,/\,k_{IIx2em}\,h]^2\,/\,\varepsilon_2$$

$$[\,0.5h_2 - 0.25\sin(2\,k_{IIx2em}\,h_2)/\,k_{IIx2em}\,] +$$

$$[\,\varepsilon_1\cos(k_{IIx1hm}\,h_1)\,/\,\varepsilon_2]^2\,/\,\varepsilon_2$$

$$[\,0.5h_2 + 0.25\sin(2\,k_{IIx2hm}\,h_2)/\,k_{IIx2hm}\,] +$$

$$[\,-k_{IIx1em}\,h\sin(k_{IIx1em}\,h_1)\,/\,k_{IIx2em}\,h_2]\,[\,\varepsilon_1\cos(k_{IIx1hm}\,h_1)$$

$$[\;\sin(k_{IIx2hm}\,h_2)]^2\,/\,\varepsilon_2\;\}^{-1/2} \qquad \text{(C-16)}$$

The othercoefficients such as N_{tII2m}, N_{rII2m} . . . can be obtained from Eqs. (C-6) to (C-13).

APPENDIX D. DERIVATION OF THE SCATTERING MARTIX FOR THE DOUBLE-STEP JUNCTION

In reference to Fig. II-3 and Eqs (II-3) to (II-24), the tangential fields in Region I can be written as

$$E_{1y} = -\partial\phi_I / \partial z + (1 / j\omega\varepsilon_o)\, \partial^2\psi_I / \partial x\partial y$$

$$= -\sum_{m=1}^{M}\sum_{n=0}^{N-1} k_{Izhmn}(-A_{Imn} + B_{Imn})\, P_{Imn} -$$

$$(1/j\omega\varepsilon_o)\sum_{m=0}^{M-1}\sum_{n=1}^{N} N_{Iemn}(mn\pi^2/a_1b_1)\, \sin(m\pi x/a_1)\, \cos(n\pi y/b_1)\, (C_{Imn} + D_{Imn}) \qquad (D\text{-}1)$$

$$E_{Ix} = (1 / j\omega\varepsilon_o)\, (\partial^2 / \partial x^2 + k_I^2)\, \psi_I$$

$$= (1/j\omega\varepsilon_o)\sum_{m=0}^{M-1}\sum_{n=1}^{N} [\, k_o^2 - (m\pi / a_1)^2]\, (C_{Imn} + D_{Imn})\, Q_{Imn} \qquad (D\text{-}2)$$

$$H_{Iy} = \partial\psi_I / \partial z + (1 / j\omega\mu_o)\, \partial^2\phi_I / \partial x\partial y$$

$$= \sum_{m=0}^{M-1}\sum_{n=1}^{N} k_{Izemn}(-C_{Imn} + D_{Imn})\, Q_{Imn} -$$

$$(1 / j\omega\mu_o)\sum_{m=1}^{M}\sum_{n=0}^{N-1} N_{Ihmn}(mn\pi^2/a_1b_1)\, \cos(m\pi x/a_1)\, \sin(n\pi y/b_1)\, (A_{Imn} + B_{Imn}) \qquad (D\text{-}3)$$

$$H_{Ix} = (1 / j\omega\mu_o)\, (\partial^2 / \partial x^2 + k_I^2)\, \phi_I$$

$$= (1/j\omega\mu_o)\sum_{m=1}^{M}\sum_{n=0}^{N-1} [\, k_o^2 - (m\pi / a_1)^2]\, (A_{Imn} + B_{Imn})\, P_{Imn} \qquad (D\text{-}4)$$

where

AD-A184 473 A STUDY OF SCATTERING FROM E-PLANE CIRCUIT ELEMENTS(U) 2/2
TEXAS UNIV AT AUSTIN MICROWAVE LAB Q ZHANG ET AL.
MAY 87 MW-87-P-5 ARO-21438.37-EL DAAG29-84-K-0076
UNCLASSIFIED F/G 9/1 NL

END

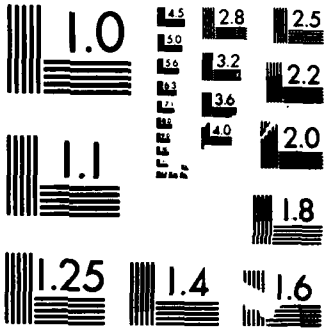

MICROCOPY RESOLUTION TEST CHART
NATIONAL BUREAU OF STANDARDS-1963-A

$$A_{Imn} = a_{Imn}\exp(-k_{Izhmn}z), \quad B_{Imn} = b_{Imn}\exp(k_{Izhmn}z)$$

$$C_{Imn} = c_{Imn}\exp(-k_{Izemn}z), \quad D_{Imn} = d_{Imn}\exp(k_{Izemn}z) \qquad (D\text{-}5)$$

In the Region II the tangential fields are given by

$$E_{IIy} = -\partial\phi_{II}/\partial z + (1/j\omega\varepsilon_o\varepsilon_j)\,\partial^2\psi_{II}/\partial x\partial y$$
$$= -\sum_{p=1}^{P}\sum_{q=0}^{Q-1} k_{IIzhpq}(-A_{IIpq} + B_{IIpq})\,P_{IIpq} + (1/j\omega\varepsilon_o)N_{vIIq}$$
$$\sum_{p=0}^{P}\sum_{q=1}^{Q}(1/\varepsilon_j(x))\,(q\pi/b)\cos[q\pi/b(y-y_1)]\,(-C_{IIpq} + D_{IIpq})\,\partial T_p/\partial x \qquad (D\text{-}6)$$

$$E_{IIx} = (1/j\omega\varepsilon_o\varepsilon_j)\,(\partial^2/\partial x^2 + k_{IIj}^2)\,\psi_{II}$$
$$= (1/j\omega\varepsilon_o)\sum_{p=0}^{P-1}\sum_{q=1}^{Q}(k_{IIj}^2 - k_{IIxjep}^2)\,(C_{IIpq} + D_{IIpq})\,Q_{IIpq}/\varepsilon_j(x) \qquad (D\text{-}7)$$

$$H_{IIy} = \partial\psi_{II}/\partial z + (1/j\omega\mu_o)\,\partial^2\phi_{II}/\partial x\partial y$$
$$= \sum_{p=0}^{P-1}\sum_{q=1}^{Q} k_{IIzepq}(-C_{IIpq} + D_{IIpq})\,Q_{IIpq} -$$
$$(1/j\omega\mu_o)\sum_{p=1}^{P}\sum_{q=0}^{Q} N_{IIsq}(q\pi/b)\sin[q\pi/b(y-y_1)]\,(A_{IIpq} + B_{IIpq})\,\partial R_p/\partial x \qquad (D\text{-}8)$$

$$H_{IIx} = (1/j\omega\mu_o)\,(\partial^2/\partial x^2 + k_{II}^2)\,\phi_{II}$$
$$= (1/j\omega\mu_o)\sum_{p=1}^{P}\sum_{q=0}^{Q}(k_{IIj}^2 - k_{IIxjhp}^2)\,(A_{IIpq} + B_{IIpq})\,P_{IIpq} \qquad (D\text{-}9)$$

where

$$A_{IIpq} = a_{IIpq}\exp(-k_{IIzhpq}z), \quad B_{IIpq} = b_{IIpq}\exp(k_{IIzhpq}z)$$

$$C_{IIpq} = c_{IIpq}\exp(-k_{IIzepq}z), \quad D_{IIpq} = d_{IIpq}\exp(k_{IIzepq}z) \qquad \text{(D-10)}$$

Match the tangetial fielde at $z = 0$ and in area A_2 leads to

$$\sum_{m=0}^{M-1}\sum_{n=1}^{N}[k_o^2 - (m\pi/a_1)^2](c_{Imn}+d_{Imn})Q_{Imn} = \sum_{p=0}^{P}\sum_{q=1}^{Q}[(q\pi/b)^2 - k_{IIzjep}^2](c_{IIpq}+d_{IIpq})Q_{IIpq}/\varepsilon_j(x) \qquad \text{(D-11)}$$

$$\sum_{m=1}^{M}\sum_{n=0}^{N-1}k_{Izhmn}(-a_{Imn}+b_{Imn})P_{Imn} + (1/j\omega\varepsilon_o)\sum_{m=0}^{M}\sum_{n=1}^{N}N_{Iemn}(mn\pi^2/a_1b_1)\sin(m\pi x/a_1)\cos(n\pi y/b_1)(c_{Imn}+d_{Imn}) = \sum_{p=1}^{P}\sum_{q=0}^{Q-1}k_{IIzhpq}(-a_{IIpq}+b_{IIpq})P_{IIpq} - (1/j\omega\varepsilon_o)\cdot N_{vIIq}\cdot \sum_{p=0}^{P-1}\sum_{q=1}^{Q}(q\pi/b)\cos[q\pi/b(y-y_1)](-c_{IIpq}+d_{IIpq})\partial T_p/\partial x/\varepsilon_j(x) \qquad \text{(D-12)}$$

$$\sum_{m=1}^{M}\sum_{n=0}^{N-1}[k_o^2 - (m\pi/a_1)^2](a_{Imn}+b_{Imn})P_{Imn} = \sum_{p=1}^{P}\sum_{q=0}^{Q-1}[(q\pi/b)^2 - k_{IIzjep}^2](a_{IIpq}+b_{IIpq})P_{IIpq} \qquad \text{(D-13)}$$

$$\sum_{m=0}^{M-1}\sum_{n=1}^{N} k_{IIzepq}(-c_{Imn} + d_{Imn})\, Q_{Imn} -$$

$$(1/j\omega\mu_o)\sum_{m=1}^{M}\sum_{n=0}^{N-1} N_{Ihmn}(mn\pi^2/a_1 b_1)\cos(m\pi x/a_1)\sin(n\pi y/b_1)\,(a_{Imn}+b_{Imn})$$

$$=\sum_{p=0}^{P-1}\sum_{q=1}^{Q} k_{IIzepq}(-c_{IIpq} + d_{IIpq})\, Q_{IIpq} -$$

$$(1/j\omega\mu_o)\sum_{p=1}^{P}\sum_{q=0}^{Q} N_{sIIq}(q\pi/b)\sin[q\pi/b(y-y_1)]\,(a_{IIpq}+ b_{IIpq})\partial R_p/\partial x$$

(D-14)

After applying the orthogonality of the eigenfunctins, following equations are obtained

$$\sum_{m=1,n=0}^{M\ N-1} M_{aI}(m,n,p,q)a_{Imn} - V_{bII}(p,q)b_{IIpq} = -\sum_{m=1,n=0}^{M\ N-1} M_{aI}(m,n,p,q)\, b_{Imn} + V_{bII}(p,q)\, a_{IIpq}$$

(D-15)

$$-\sum_{p=0,q=1}^{P-1\ Q} M_{dII}(m,n,p,q)d_{IIpq} + V_{cI}(m,n)c_{Im} = \sum_{p=0,q=1}^{P-1\ Q} M_{dII}(m,n,p,q)\, c_{IIpq} - V_{cI}(m,n)\, d_{Imn}$$

(D-16)

$$\sum_{m=1,n=0}^{M\ N-1} M_{bI}(m,n,p,q)a_{Imn} + \sum_{m=0,n=1}^{M-1\ N} M_{cI}(m,n,p,q)\, c_{Imn} - V_{aII}(p,q)\, b_{IIpq} + V_{dII}(p,q)\, d_{IIpq}$$

$$= -\sum_{m=1,n=0}^{M\ N-1} M_{bI}(m,n,p,q)b_{Imn} + \sum_{m=0,n=1}^{M-1\ N} M_{cI}(p,n,p,q)d_{Imn} + V_{aII}(p,q)a_{IIpq} + V_{dII}(p,q)\, c_{IIpq}$$

(D-17)

$$\sum_{p=1,q=0}^{P\ Q-1} M_{bII}(p,q,m,n)\, b_{IIp} + \sum_{p=0,q=1}^{P-1\ Q} M_{cII}(p,q,m,n)\, d_{IIpq} V_{aI}(m,n)a_{Im} - V_{dI}(m,n)\, c_{Imn}$$

$$=\sum_{p=1,q=0}^{P\ Q-1} M_{bII}(p,q,m,n)\, a_{IIp} - \sum_{p=0,q=1}^{P-1\ Q} M_{cII}(p,q,m,n)\, c_{IIpq} + V_{aI}(m,n)\, b_{Imn} + V_{dI}(m,n)\, d_{Imn}$$

(D-18)

where

$$M_{aI}(m,n,p,q) = [\, k_o^2 - (m\pi / a_1)^2] \int_{y_1}^{y_1+b} dy \int_{x_1}^{x_1+a} dx\, P_{Imn}(x,y)\, P_{IIpq}(x,y)$$

$$M_{dII}(m,n,p,q) = [\, (q\pi/b)^2 - k_{IIzepq}^2] \int_{y_1}^{y_1+b} dy \int_{x_1}^{x_1+a} dx\, Q_{Imn}(x,y)\, Q_{IIpq}(x,y) / \varepsilon_j(x)$$

$$M_{bI}(m,n,p,q) = N_{Ihmn} mn\pi^2/(a_1 b_1\, j\omega\mu_o\, N_{Iemn}) \int_{y_1}^{y_1+b} dy \int_{x_1}^{x_1+a} dx\, Q_{Imn}(x,y)\, Q_{IIpq}(x,y) / \varepsilon_j(x)$$

$$M_{cI}(m,n,p,q) = k_{Izemn} \int_{y_1}^{y_1+b} dy \int_{x_1}^{x_1+a} dx\, Q_{Imn}(x,y)\, Q_{IIpq}(x,y) / \varepsilon_j(x)$$

$$M_{bII}(m,n,p,q) = k_{IIzhpq} \int_{y_1}^{y_1+b} dy \int_{x_1}^{x_1+a} dx\, Q_{Imn}(x,y)\, Q_{IIpq}(x,y)$$

$$M_{cII}(m,n,p,q) = N_{vIIq} q\pi / (j\omega\varepsilon_o b) \int_{y_1}^{y_1+b} dy \int_{x_1}^{x_1+a} dx \cos[q\pi/b(y-y_1)\, P_{Imn}(x,y) \partial T_{IIp}(x) / \partial x / \varepsilon_j(x)$$

$$V_{bII}(p,q) = (q\pi/b)^2 - k^2_{IIzepq}$$

$$V_{cI}(m,n) = k_o^2 - (m\pi / a_1)^2$$

$$= (q\pi/b)^2 - k^2_{IIzepq}$$

$$V_{aII}(p,q) = N_{sIIq} q\pi / (j\omega\mu_o b) \int_{y_1}^{y_1+b} dy \int_{x_1}^{x_1+a} dx \sin[q\pi/b(y-y_1)\, Q_{IIpq}(x,y) \partial R_{IIp}(x,) / \partial x / \varepsilon_j(x)$$

$$V_{bII}(p,q) = k_{IIzepq}$$

$$V_{aI}(m,n) = k_{IIzhmn}$$

$V_{dII}(m,n) = mn\pi^2/(a_1 b_1 j\omega\varepsilon_o)$

Equations (D-15) to (D-18) may be written in matrix form

$$\begin{pmatrix} Ma_I & 0 & -V_{bII} & 0 \\ 0 & V_{cI} & 0 & -M_{dII} \\ M_{bI} & M_{cI} & -V_{aII} & V_{dII} \\ V_{aI} & -V_{dI} & M_{bII} & M_{cII} \end{pmatrix} \begin{pmatrix} A_{Imn} \\ C_{Imn} \\ B_{IIpq} \\ D_{IIpq} \end{pmatrix} = \begin{pmatrix} -M_{aI} & 0 & V_{bII} & 0 \\ 0 & -V_{cI} & 0 & M_{dII} \\ -M_{bI} & M_{cI} & V_{aII} & V_{dII} \\ VaI & V_{dI} & M_{bII} & -M_{cII} \end{pmatrix} \begin{pmatrix} B_{Imn} \\ D_{Imn} \\ A_{IIpq} \\ C_{IIpq} \end{pmatrix} \quad (D\text{-}19)$$

where M_{aI} is a matrix of dimension of PxQxMxN and is given by :

$$M_{aI} = \begin{pmatrix} M_{aI}(1,0,1,0), M_{aI}(1,0,1,1) \ldots M_{aI}(1,0,M,N-2), M_{aI}(1,0,M,N-1) \\ M_{aI}(1,1,1,0), M_{aI}(1,1,1,1) \ldots M_{aI}(1,1,M,N-2), M_{aI}(1,1,M,N-1) \\ \vdots \\ M_{aI}(2,0,1,0), M_{aI}(2,0,1,1) \ldots M_{aI}(2,0,M,N-2), M_{aI}(2,0,M,N-1) \\ M_{aI}(2,1,1,0), M_{aI}(2,1,1,1) \ldots M_{aI}(2,1,M,N-2), M_{aI}(2,1,M,N-1) \\ \vdots \\ M_{aI}(P,Q-2,1,0), M_{aI}(p,Q-2,1,1) \ldots M_{aI}(\ldots), M_{aI}(P,Q-2,M,N-1) \\ M_{aI}(P,Q-1,1,0), M_{aI}(p,Q-1,1,1) \ldots M_{aI}(\ldots), M_{aI}(P,Q-1,M,N-1) \end{pmatrix}$$

The dimensions of matrix M_{dII}, M_{bI}, M_{cI}, M_{bII}, and M_{cII} are PxQxPxQ, MxNxMxN, MxNxMxN, MxNxPxQ, and MxNxPxQ, respectively. The V_{bII} is a diagonal matrix of PxQxPxQ. It is represented by

$$V_{bII} = \begin{bmatrix} V_{II}(0,0) & 0 & 0 & \cdots & 0 & 0 \\ 0 & V_{bII}(1,1) & 0 & \cdots & 0 & 0 \\ 0 & & V_{bII}(2,2) & & & 0 \\ \vdots & & \ddots & & \vdots & \vdots \\ & & & \ddots & \vdots & \vdots \\ & & & & \ddots & 0 \\ 0 & & & & V_{bII}(Q-2,Q-2) & 0 \\ 0 & 0 & 0 & & \cdots & V_{bII}(Q-1,Q-1) \end{bmatrix}$$

Other diagonal matrices such as V_{cI}, V_{aI}, V_{bII} ...etc. may be obtained similarly. In Eg. (D-19), A_{Imn} , D_{IIpq} , ... are the coefficient vectors of dimensions of MxN, Px Q,... and so on. For instance, A_{Imn} is a vector of dimension of MxN and is givenby

$$A_{Imn} = [\, a_{I10}, a_{I11}, \cdots, a_{I20}, a_{I21}, \cdots, a_{Im(n-2)} , a_{Im(n-1)}]^{T}$$

where T indicates a transpose operation.

APPENDIX E. DERIVATION OF SCATTERING MATRIX FOR THE CASCADED DISCONTINUITIES

From Fig. II-10, the following matrix equations can be derived:

$$\begin{pmatrix} R^{(A)} \\ R^{(2)} \end{pmatrix} = \begin{pmatrix} S_{f111} & S_{f112} \\ S_{f121} & S_{f122} \end{pmatrix} \begin{pmatrix} I^{(A)} \\ I^{(2)} \end{pmatrix} \qquad (E\text{-}1)$$

$$\begin{pmatrix} I^{(2)} \\ I^{(3)} \end{pmatrix} = \begin{pmatrix} 0 & S_t \\ S_t & 0 \end{pmatrix} \begin{pmatrix} I^{(2)} \\ I^{(3)} \end{pmatrix} \qquad (E\text{-}2)$$

$$\begin{pmatrix} R^{(3)} \\ R^{(C)} \end{pmatrix} = \begin{pmatrix} S_{f111} & S_{f112} \\ S_{f121} & S_{f122} \end{pmatrix} \begin{pmatrix} I^{(3)} \\ I^{(C)} \end{pmatrix} \qquad (E\text{-}3)$$

Equation (E-2) is substituted into (E-1) to obtain

$$R^{(A)} = S_{f111}\, I^{(A)} + S_{f112}\, S_t\, R^{(3)} \qquad (E\text{-}4)$$

$$R^{(2)} = S_{f121}\, I^{(A)} + S_{f122}\, S_t\, R^{(3)} \qquad (E\text{-}5)$$

Next, (E-2) is substituted into (E-3) to get

$$R^{(3)} = S_{f211}\, S_t\, R^{(2)} + S_{f212}\, I^{(C)} \qquad (E\text{-}6)$$

$$R^{(C)} = S_{f221}\, S_t\, R^{(2)} + S_{f222}\, I^{(C)} \qquad (E\text{-}7)$$

Equations (E-5) and (E-6) are used to isolate $R^{(2)}$ and $R^{(3)}$:

$$R^{(2)} = U_1 S_{f121} I^{(A)} + U_1 S_{f122} S_t \; S_{f212} I^{(C)} \qquad (E\text{-}8)$$

$$R^{(3)} = U_2 S_{f211} S_t \; S_{f121} I^{(A)} + U_2 S_{f212} I^{(A)} \qquad (E\text{-}9)$$

where

$$U_1 = (I - S_{f122} S_t S_{f211} S_t)^{-1} \qquad (E\text{-}10)$$

$$U_2 = (I - S_{f211} S_t S_{f121} S_t)^{-1} \qquad (E\text{-}11)$$

Where I is the identity matrix. Finally, equations (E-8) and (E-9) are substituted into equations (E-4) and (E-7)

$$R^{(A)} = [S_{f111} + S_{f112} S_t U_2 S_{f211} S_t \; S_{f121}] I^{(A)} + S_{f112} S_t U_2 \; S_{f212} I^{(C)} \qquad (E\text{-}12)$$

$$R^{(C)} = S_{f221} S_t U_1 \; S_{f121} I^{(A)} + [S_{f222} + S_{f221} S_t U_1 S_{f122} S_t \; S_{f212}] I^{(C)} \qquad (E\text{-}13)$$

The submatrixes S_{AA}, S_{AC}, S_{CA}, and S_{CC} are easily idetified from the above equations.

REFERENCES OF PART ONE

[1] P. J. Meier, "Two new integrated-circuit media with special advantages at millimeter wavelengths," IEEE-GMTT International Microwave Symposium Digest, pp.221-223, 1972.

[2] P. J. Meier, "Integrated fin-line millimeter components," IEEE Trans. Microwave Theory Tech., Vol.MTT-22, pp.1209-1216, Dec. 1974.

[3] Y. Konishi, K. Uenakada and N.Hoshino, "The design of planar circuit mounted in waveguide and the application to low noise 12-GHz converter," IEEE S-MTT International Microwave Symposium Digest, pp.168-170, 1974.

[4] Y. Konishi and K. Uenakada, "The design of a bandpass filter with inductive strip-planar circuit mounted in waveguide," IEEE Trans. Microwave Theory Tech., Vol.MTT-22, pp.869-873, Oct. 1974.

[5] Y. Konishi, "Planar circuit mounted in waveguide used as a downconverter," IEEE Trans. Microwave Theory and Tech., Vol.MTT-26, pp.716- 19, Oct. 1978.

[6] Y.C. Shih, T. Itoh and L. Bui, "Computer-aided design of millimeter- wave E-plane filter," IEEE Trans. Microwave Theory Tech., Vol.MTT-31, pp.135-141, Feb. 1983.

[7] K. Chang and P.J. Khan, "Equivalent circuit of a narrow axial strip in waveguide," IEEE Trans. Microwave Theory Tech., Vol.MTT-24, pp.611-615, Sept. 1976.

[8] R. Collin, Field Theory of Guided Waves, New York McGROW-Hill, 1960, pp.224-232.

[9] T. Itoh, "Spectral domain immittance approach for dispersion characteristics of generalized printed transmission lines," IEEE Trans. Microwave Theory Tech., Vol.MTT-28, pp.733-736, July 1980.

[10] R. Mittra and S. W. Lee, Analytical Techniques in the Theory of Waveguide Waves, New York: Macmillan, 1971, pp. 4-11.

REFERENCES OF PART TWO

[1] E. T. Jaynes, "Ghost Modes in Imperfect waveguides," Proc.IRE, Vol.46, pp.416-418, Feb. 1958.

[2] W. A. Edson, "Microwave Filters Using Ghost-Mode Resonance," IRE Electron. Components Conf., Vol. 19, pp. 2, 1961.

[3] G. Craven , "Waveguide Band-pass Filters Using Evanescent Modes," Electro Lett. Vol. 2, pp.251- 252, 1966.

[4] G. Craven and C.K.Mok, "The Design of Evanescent Mode Waveguide Band-pass Filters for a Prescribed Insertion Loss Characteristic," IEEE Trans. Microwave Theory Tech. Vol. MTT-19, pp. 295-308, March 1971.

[5] R. Snyder, "New Application of Evanescent Mode Waveguide to Filters Design," IEEE Trans. Microwave Theory Tech. Vol. MTT-25 pp. 1013-1021, Dec. 1977.

[6] C.K. Mok, "Diaphragms in Evanescent Waveguides," Electro Lett. Vol. 4, pp. 43-44, Feb. 1968.

[7] Q. Zhang and T. Itoh, "Spectral- Domain Analysis of Scattering from E-plane Circuit Elements," IEEE Trans. Microwave Theory Tech. Vol. MTT-35 pp. 138-150, Feb. 1987.

[8] S.B. Cohn, "Direct-coupled-Resonator Filters," Proceedings of the IRE, Vol. No.2, pp. 187-196, Feb. 1957.

[9] G. L. Mattaei, L.Young, and E. M. T. Jones, Microwave Filters, Impedance-Matching Networks, and Coupling Structures. New York: McGraw-Hill, 1964, Chapter 8.

[10] J. Pace and R. Mittra, "Generalized Scattering Matrix Analysis of Waveguide Discontinuity Problem," Quasi-Optics XIV, Polytechnic Institut of Brookline Press, NY. pp. 172-194, 1964.

[11] R. Mittra and S.W. Lee, Analytical Techniques in the Theory of Guided Waves, New York : Macmillan, 1971, pp. 207-217.

[12] H. Patzelt and F. Arndt, "Double-Plane Steps in Rectangular Waveguide and their Application for Transformer, Irises, and Filters," IEEE Trans. Microwave Theory Tech. Vol. MTT-30 pp. 771-776, May 1982.

[13] T.K. Chu, T. Itoh and Y.C. Shih, "Comparative Study of Mode-Matching for Microstrip Discontinuity Problems," IEEE Trans. Microwave Theory Tech. Vol. MTT-33, pp. 1018-1023, Oct.1985.

[14] R. F. Harrington, Time-Harmonic Electromagnetic Fields, New York, McGraw-Hill, 1968.

[15] F. Arndt and T.Wriedt, "Computer-Optimized Multisection Transformers between Rectangular Waveguide of Adjacent Frequency Bands," IEEE Trans. Microwave Theory Tech. Vol. MTT-32 pp. 1479-1484, Nov. 1984.

[16] Y. C. Shih, T. Itoh, and L. Q. Bui, " Computer-Aided Design of Millimeter Wave E-Plane Filter," IEEE Trans. Microwave Theory Tech. Vol. MTT-31 pp. 135-142, Feb. 1983.

END

10-81

DTIC